University of Alberta

Exchange Flow Through an Opening

By

Yaw Anim Okyere

A thesis submitted to the Faculty of Graduate Studies and Research in partial fulfillment of the requirements for the degree of **Master of Science**

in

Water Resources Engineering

Department of Civil and Environmental Engineering

Edmonton, Alberta

Spring 2000

National Library of Canada
Acquisitions and Bibliographic Services
395 Wellington Street
Ottawa ON K1A 0N4
Canada

Bibliothèque nationale du Canada
Acquisitions et services bibliographiques
395, rue Wellington
Ottawa ON K1A 0N4
Canada

Your file Votre référence

Our file Notre référence

The author has granted a non-exclusive licence allowing the National Library of Canada to reproduce, loan, distribute or sell copies of this thesis in microform, paper or electronic formats.

L'auteur a accordé une licence non exclusive permettant à la Bibliothèque nationale du Canada de reproduire, prêter, distribuer ou vendre des copies de cette thèse sous la forme de microfiche/film, de reproduction sur papier ou sur format électronique.

The author retains ownership of the copyright in this thesis. Neither the thesis nor substantial extracts from it may be printed or otherwise reproduced without the author's permission.

L'auteur conserve la propriété du droit d'auteur qui protège cette thèse. Ni la thèse ni des extraits substantiels de celle-ci ne doivent être imprimés ou autrement reproduits sans son autorisation.

0-612-60162-5

Canada

University of Alberta

Library Release Form

Name of Author:	Yaw Anim Okyere
Title of Thesis:	Exchange Flow Through an Opening
Degree:	Master of Science
Year this Degree Granted:	2000

Permission is hereby granted to the University of Alberta Library to reproduce single copies of this thesis and to lend or sell such copies for private, scholarly, or scientific research purposes only.

The author reserves all other publication and other rights in association with the copyright in the thesis, and except as herein before provided, neither the thesis nor any substantial portion thereof may be printed or otherwise reproduced in any material form whatever without the author's prior written permission.

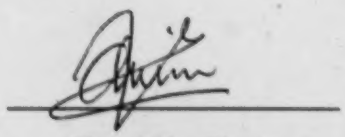

Yaw Anim Okyere
P. O. Box 490
Tema, Ghana

Date: 9th Nov. 1999

University of Alberta

Faculty of Graduate Studies and Research

The undersigned certify that they have read, and recommend to the Faculty of Graduate Studies and Research for acceptance, a thesis entitled *Exchange flow Through an Opening*, submitted by *Yaw Anim Okyere* in partial fulfillment of the requirements for the degree of *Master of Science* in *Water Resources Engineering*.

Dr. D. Z. Zhu
(Supervisor)

Dr. N. Rajaratnam
(Committee Chair & Examiner)

Dr. S. Liu
(Committee Member)

Date: Nov 9/99

ABSTRACT

Two-layer exchange flow through an opening was studied experimentally. The study adopted a planar sluice gate situated in a rectangular channel. The exchange flow was created by connecting two reservoirs with fluids of different densities in the rectangular channel. Density driven flows were first investigated, followed by barotropic forcing which was created by pumping the denser fluid from one reservoir to another.

The interface of the two layers was distinguished by mixing Sodium Flouresceine dye to the reservoir containing denser fluid. Flow velocity fields were obtained by adding neutrally buoyant tracer particles into the fluid. The movements of the tracer particles and the interface position were recorded simultaneously. The recorded images were analyzed using particle tracking and image processing techniques.

The critical points or hydraulic controls of exchange flows where the composite Froude number is unit were identified experimentally. Contradiction to the predictions of traditional hydraulic theories, the experimental results reveal a shift of the control location due to barotropic forcing. This study is therefore important in understanding the control mechanisms of skimmer walls, which are often used in the selective withdrawal of cold water from thermally stratified reservoirs. The results are also applicable to the exchange of warm and cold air through doorways or windows as well as the operation of navigation locks.

Acknowledgement

I am very grateful to everyone at the Thomas Blench Hydraulics Laboratory in University of Alberta, Edmonton. I wish to register my sincere thanks to Dr. David Zhu, who has been my supervisor throughout this thesis period.

The review towards this thesis would not have been successful without my knowledge in hydraulics and hydrology; it is therefore very important for me also to thank Dr. N. Rajaratnam, Dr. P. M. Steffler, Dr. F. E. Hicks and Dr. T. Gan for taking me through a series of courses in Water Resources Engineering.

My special thanks also go to Mr. S. Lovell and Mr. P. Fedun. Their invaluable practical support made me realize this piece of work.

Yaw Anim Okyere

November 1999

TABLE OF CONTENTS

Page

Abstract

Acknowledgement

List of Figures

List of Tables

List of Symbols and Definitions

Chapter 1: Introduction 1

Chapter 2: Literature Review 4

2.1 Hydraulics of Single-layer Flow under a Sluice Gate 4

2.2 Hydraulics of Exchange Flows 5

2.3 Two-layer Flow through an Opening 7

Chapter 3: Equation Derivations 12

3.1 Internal Hydraulics 12

3.2 Prediction of Flow Rate 16

Chapter 4: Experimental Apparatus and Techniques 19

4.1 Experimental Design and Set-up 19

4.2 Experimental Preparation 24

4.3 Velocity and Interface Position Measurements 25

Chapter 5: Experimental Results and Discussions 28

5.1 Non-barotropic Experiments 28

5.1.1 Evolution of the Flow 28

5.1.2 Measurements of Flow Rate and Interface positions 30

5.1.3 Composite Froude Number 37

5.2 Barotropic Forcing Experiments without Exit Control 43

5.3 Barotropic Forcing Experiments with Elevated Channel Bed 49

5.4 Detailed Results of all the Experiments 58

Chapter 6: Application of Two-layer Exchange Flow through an Opening in Engineering 61

6.1 Exchange Flow through Windows and Doorways 61

6.2 Navigation Lock Operations 62

6.3 Selective Withdrawal of Cold Water using Skimmer Walls 62

Chapter 7: Conclusions 64

References 66

Appendix A: Variation of Flow Rate and Interface Positions 69

List of Figures

Figure		Page
2.1	Flow without barotropic forcing	7
2.2	Flow under a skimmer wall	8
2.3	Flows through doorways and windows with net flow	8
3.1	Two-layer flow over a smooth sill	12
3.2	Exchange flow through an opening	16
4.1	Plan and side view of the experimental set-up	21
4.2	Chart for salt water density estimation	24
5.1	Regimes of exchange flow without barotropic forcing	29
5.2	Flow rate curve for experiment #3	31
5.3	Comparison of flow rates for the non-barotropic forcing experiments	32
5.4	Streak photograph taken with an exposure time of ¼ of a second to portray the flow pattern in the upper layer	33
5.5	Averaged interface positions and effective upper layer flow surface for experiment #3 with gate opening *d=17cm and H=30cm*	34
5.6	Interface positions with time at the gate and channel exit for Experiment #3 having gate opening *d=17cm* and *H=30cm.*	35
5.7	Variation of internal energy (E) for experiment #3	36
5.8	Streak photograph to portray the flow pattern beyond the gate	36
5.9(a)	Plot of Froude numbers for the upper and the lower layers for experiment #3 having gate opening *d=17cm* and *H=30cm.*	37
5.9(b)	Composite Froude number for experiment #1	38
5.10	Composite Froude number for experiment #2	38

5.11	Composite Froude number for experiment #3	39
5.12	Composite Froude number for experiment #4	39
5.13	Composite Froude number for experiment #5	40
5.14	Composite Froude number for experiment #6	40
5.15	Plot of composite Froude number versus d/H	42
5.16	Variation of flow rate for experiment #7	44
5.17	Variation of interface positions for experiment #7	45
5.18	Froude numbers for the upper and the lower layers for experiment #7	45
5.19	Composite Froude number for experiment #7	46
5.20	Composite Froude number for experiment #8	47
5.21	Composite Froude number for experiment #9	47
5.22	Streak photograph for experiment #11	49
5.23	Streak photograph of experiment #12 showing the flow past the free overfall	51
5.24	Variation of flow rate for experiment #11	51
5.25	Interface positions for experiment #11	52
5.26	Froude number of the upper and lower layers for experiment #11	53
5.27	Composite Froude number for experiment #11	53
5.28	Composite Froude number for experiment #10	54
5.29	Composite Froude number for experiment #12	54
5.30	Composite Froude number for experiment #13	55
5.31	Variation of flow rate for experiment #12	56
5.32	Streak photograph showing arrested flow for experiment #12	57
5.33	Interface positions versus internal energy for experiment #12	57

List of Tables

4.1	Non-barotropic experiments	23
4.2	Barotropic forcing experiments without exit control	23
4.3	Barotropic forcing experiments with elevated channel bed	23
5.1	Hydraulic parameters of non-barotropic forcing experiments	58
5.2	Hydraulic parameters of barotropic forcing experiments without exit control	58
5.3	Hydraulic parameters of barotropic forcing experiments with elevated channel	59

List of Symbols and Definitions

b	width of the rectangular channel connecting the reservoirs
d	sluice gate opening
E	internal energy for two-layer flow
$F_i^2 = q_i^2 / g' y_i^3$	densimetric Froude number for layer i
F_{1o}^2	densimetric Froude number in the upper layer at the gate
F_{2o}^2	densimetric Froude number in the lower layer at the gate
F_{1e}^2	densimetric Froude number in the upper layer at the channel exit
F_{2e}^2	densimetric Froude number in the lower layer at the channel exit
$G^2 = F_1^2 + F_2^2$	composite (or internal) Froude number
g	gravitational acceleration
$g' = \left(1 - \rho_1 / \rho_2\right) g$	reduced gravitational acceleration
h_O	gate submergence (height of the sharp sill)
h	height of topography
H	total depth of flow
ΔH	differential head
L	length of the rectangular channel in the test region
P	pressure
P^*	piezometric pressure

$q = \frac{Q}{b}$	flow rate per unit width of channel
q_i	flow rate per unit width of channel in layer i
Q_i	volumetric flow rate in layer i
$r = \rho_1 / \rho_2$	relative density difference
$R_e = \frac{q}{\nu}$	Reynolds number
S_c	curvature slope
S_f	friction slope
S_0	topographic slope
t	time
$U_i = q_i / y_i$	horizontal mean velocity in layer i
x	horizontal coordinate (with the origin at the sluice gate location)
y_b	depth of flow at the brink for single layer flow
y_c	critical depth for single layer flow
y_i	thickness of layer i
y_{1o}	thickness of the upper layer at the sill or gate
y_{2o}	thickness of the lower layer at the sill or gate
y_{1e}	thickness of the upper layer at the exit of channel
y_{2e}	thickness of lower layer at the exit of channel
ρ_i	density of layer i
ν	kinematic viscosity

Chapter 1

INTRODUCTION

When two bodies of fluids of slightly different densities are connected by a channel flow starts to exchange. Such exchange flows are common in nature; for example the exchange of more saline Mediterranean sea water with less saline Atlantic Ocean water through the Strait of Gibraltar (Armi & Farmer, 1986) and the summertime exchange of warmer, heavily polluted Hamilton Harbor water with cooler (more dense) Lake Ontario water through the Burlington ship canal (Hamblin & Lawrence,1990).

The exchange of flow of slightly different densities in a channel with an opening like a sluice gate or a lock gate is important in numerous engineering problems (Adams & Cosler, 1988). Whiles such flows may have initial local disturbances as a result of gate operation for instance, the predominant effect as outlined by Barr(1963) will be a continuing exchange flow pattern.

In situations where there is no net flow, the flow rate of the denser fluid is balanced by that of the less dense fluid with the denser layer flowing beneath the lighter layer. However, in two-layer exchange flows, it is also possible to have a net flow due to external forcing. This is called barotropic forcing such as meteorological effects in the atmosphere or tides in oceans. In much the same way imposed flows in channels as a result of water level difference or forced flow rate also results in barotropic forcing. Applications of flow involving barotropic forcing include selective withdrawal of cold water from stratified reservoir using skimmer wall (Harleman et al, 1958; Harleman & Elder 1965), the prevention of mixing in cooling canals used in process engineering

(Adams & Cosler, 1988) and the design of quarantine wards in hospitals (Shaw & Whyte, 1974).

Most of the previous investigations on two-layer flows with sudden obstructions concentrated on the position and flow conditions at points where flow is in critical condition without considering the effects such as frictional forces (see Dalziel & Lane-Serff, 1991; Jirka, 1979; Adams & Cosler, 1988). Some of the control points were theoretically imposed without actual experimental investigation to verify the magnitude of the composite Froude number especially in cases involving the introduction of a sudden obstruction like locks and sluice gates. Pratt (1986) pointed out the importance of friction in his study of two-layer flow over a topography with a stagnant the upper layer. Zhu & Lawrence (1999) have shown in their studies on two-layer flow over a smooth sill that the control point can shift from sill crest as a result of friction and non-hydrostatic forces.

The motivation of this study is to bring an understanding to the mechanisms which control the flow as well to evaluate the composite Froude number for different flow situations. The study focuses on the experimental investigation of exchange flows with and without barotropic effects through a sudden opening formed with a planar sluice gate. This experimental study requires simultaneous measurement of the individual layer thickness as well as the velocity field in each layer for the different flow situations. The study will help in understanding the movement of air through a fully or partially opened doorway with and without the influence of forcing to ascertain the amount of supply air required to prevent this movement. It will apply in navigation lock operation where the

lock needs to be lifted with minimal movement of water from the different lock chambers where the density is different.

Chapter 2 reviews the hydraulics of single layer and two-layer flow through an opening. Chapter 3 reviews the derivation of internal hydraulic theory for two-layer flow over a smooth sill. The equations to predict flows for irrotational, inviscid flows through openings where non-hydrostatic forces are negligible are then presented.

Chapter 4 discusses the experimental set-up, the procedure and the measurement of the velocity field and interface positions using particle tracking and image processing techniques. Dimensional analysis of various parameters of interest together with lists of experiments are presented.

Results of the experimental study are presented in Chapter 5. Tables giving complete summary of all the flow situations and plots of sample curves showing the variations in flow rate, interface positions and Froude number can be found in this chapter. A complete list of all the measured hydraulic parameters at steady state for the various experimental runs are also presented in this chapter. Factors such as interfacial mixing, streamline curvature and wall friction have been discussed. Their effects on the accuracy of the experiments have also been pointed out.

The engineering applications of two-layer exchange flow through openings such as sluice gates are discussed in Chapter 6 and conclusions are summarized in Chapter 7.

Chapter 2

LITERATURE REVIEW

For the purpose of this experimental study, a planar sluice gate was adopted. It was found necessary to know about what has been done for single layer flows under a sluice gate so that the ideas can be borne in mind in dealing with two-layer flows. This chapter therefore gives a brief review of single-layer flows under sluice gates as well as two-layer flows through openings.

2.1 Hydraulics of Single-layer Flows under a Sluice Gate

The use of sluice gates to regulate flows in hydraulic structures as well as a metering device has led to many experimental and theoretical studies. Research work in this area dates back as early as the beginning of the century with notable contribution by Gibson (1918). All the previous studies schematized the flow to some degree so that they can be amenable to detailed analysis. The flow under a sluice gate which is turbulent and viscous (real fluid) is assumed to be represented sufficiently well as two-dimensional, irrotational and inviscid. Common features of all the previous analysis on planar sluice gates assume uniform flow conditions with a local horizontal surface profile which occur a relatively short distance upstream and downstream of the gate. The flow below the gate represents a transition region from subcritical to supercritical flow and again to subcritical flow (if any) through a hydraulic jump some distance downstream of the gate.

Rajaratnam & Humphries (1982), in their experimental study, pointed out the evidence of loss in the vortex region infront of the sluice gate. In their study, the geometry of the

vortex region was measured and a relationship between the geometry of the eddy region and the gate opening as well as the upstream water level were obtained using dimensional analysis. An earlier experimental study by Rajaratnam (1977) dealt with the investigation of the contraction coefficient, surface profile and pressure field in the supercritical stream below the gate. Montes (1997) also pointed out that non-hydrostatic forces as well as vortex formation can be very important for single layer flows.

2.2 Hydraulics of Exchange Flows

Previous studies on two-layer flows include the earliest work of Schijf & Schonfeld (1953) in which a survey of the theoretical investigation on the motion of salt and fresh water in estuaries and locks were presented. The continuity and the dynamical equation of two layers were used for unsteady state in which wave celerities were derived. Two-layer flows have been studied both theoretically and experimentally in laboratories using long flumes. Theoretical development of two-layer flow equations is simplified using steady state assumptions.

Two-layer flows are typically assumed to be incompressible, inviscid, irrotational, steady and uniform. Hydrostatic pressure distribution and a constant density in each layer for which the velocity varies only in the direction of flow are invoked (Lawrence, 1990). The assumption of hydrostatic pressure distribution as pointed out by Baines (1984) holds for flows where the horizontal scales are much greater than vertical scales. The fluids are also considered to have a small density difference thus rigid lid or Boussinesq's approximation can be applied. The equations for two-layer flows can be derived by using

the continuity equation for the two-layers together with either energy equation for both layers (Denton 1987; Lawrence 1993) or the steady momentum equation (Yih 1969; Baines 1984; Armi 1986; Dalziel 1991). Both approaches give the same regularity condition. The energy equation however gives a relation which represents the variation of the interface slope at any given instant under consideration except in sections of discontinuities. The combined solutions of the energy and continuity equations do not explicitly involve the direction of the flow of either layer which means that the solutions obtained are applicable to both exchange and uni-directional flows.

In two-layer flows, points where the internal Froude number is unity are called internal hydraulic controls. For a known discharge in each layer, this relationship determines the flow depths at the control and hence the layer thickness. Unlike single layer flows, two-layer flows require two control points for interface profile computation. One point is obtained at the maximum sill height or contraction based on analytical solution, which is usually described as a topographic control. The other control point will occur in a region outside the topography. This has been explained with equations in ***section 3.1***. For two-layer flows over smooth sills, the interface profile can then be computed from one control point to another either upstream or downstream provided there are no discontinuities such as internal hydraulic jumps.

There is however a shift in the location of this topographic control if other factors such as geometry, friction, streamline curvature and barotropic affects are considered (see Armi & Farmer 1986; Pratt 1986; Bormans & Garrett 1989; Zhu & Lawrence 1998). For flows through a channel containing a combination of a sill and a contraction for which both coincide, the topographic control is at the point of coincidence.

2.3 Two-layer Flow through an Opening

Two-layer flow through an opening such as sluice gates, locks, skimmer walls, windows or doorways can be broadly classified into two groups, namely, those with net flow and those without net flow. Flows without net flow results in a continuous exchange due to the difference in density and the flow rate is the same in both layers. Such flows are called non-barotropic flows. ***Figure 2.1*** illustrates a simple case where the flows are driven by density difference.

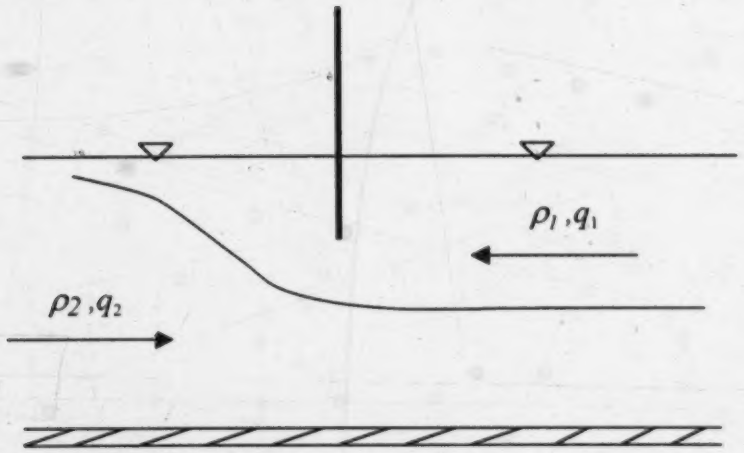

Figure 2.1 Flow without barotropic forcing. In this case $q_1 = q_2$

There are instances where flow rates in two layers can be different when there are external forcing known as barotropic forcing. Barotropic forcing can be subdivided into two. The first subdivision comprises of flows that are driven by difference in water level or head which results in a net flow as shown in ***figure 2.2***. The other group embodies all situations where there is an imposed net flow as in typical cases of flow of air in

quarantine wards and operating theatres. It is also the same for places where there is a need to expel or reduce an inflow of certain air through an opening. The sketch in ***figure 2.3*** illustrates an imposed flow through a window or doorway.

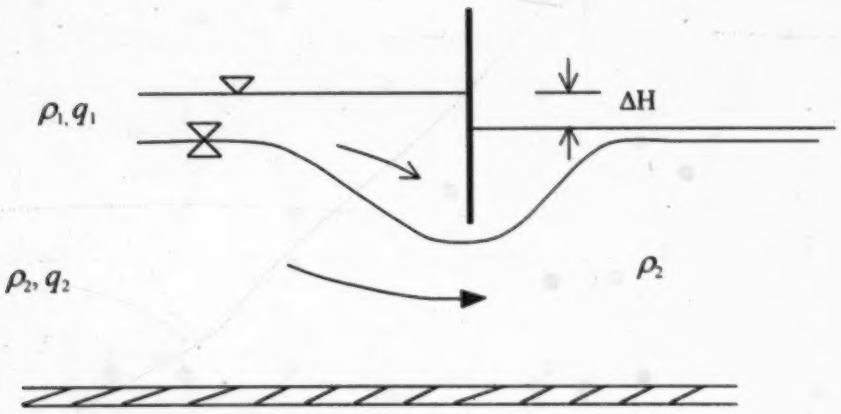

Figure 2.2 Partial lifting of the skimmer wall and the differential head results in a net flow. In this case $q_1 \neq q_2$

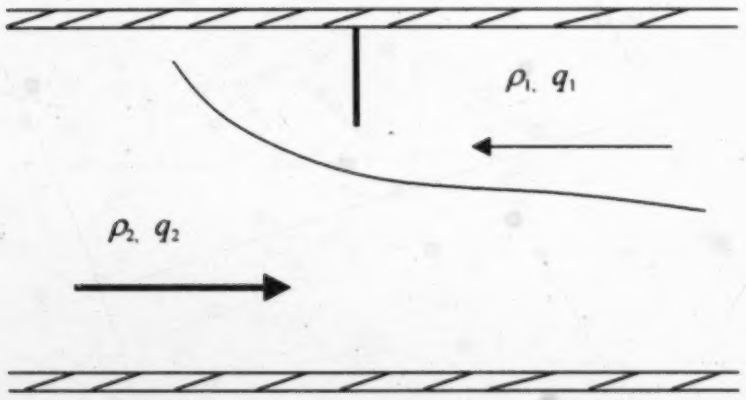

Figure 2.3 Flows through doorways and windows with net flow for which $q_1 \neq q_2$

Harleman *et al* (1958) did the earliest work on skimmer walls with the objective of finding solutions to the increasing demand of cold water from a stratified reservoir for thermal plant cooling. The idea of establishing the conditions for maximum discharge from the lower heavier layer without withdrawal of the lighter layer above was pointed out. The effects of streamline curvature and the presence of separation wedge behind the skimmer wall just after the point of incipient motion were taken into consideration by introducing the Khafagi-Hammad functions. In a later paper of Harleman & Elder (1965), one-dimensional energy equation was formulated between a point well upstream from the skimmer wall where the flow velocities are negligible and a point just downstream from the skimmer wall opening.

Barr (1963; 1967) and Barr & Hassan (1963) in an attempt to answer questions relating to the phenomenon of exchange flow in water and the scaling effects of hydraulic models, conducted series of experiments with rectangular channels containing lock gate separating fluids of different densities. Dimensional analysis was also carried out for both circular and rectangular channels. Although it was pointed out that the mechanism of lock exchange flow changes considerably with scale, the velocity measurements in their experimental studies were not reliable.

In their study of selective withdrawal of cooler water from a stratified reservoir, Lohmeyer & Plate (1977) recognized the fact that energy loss as reflected in the formation of the velocity profiles was very important. The effect of friction was considered using the resistance on a thin plate, which was pulled through a fluid at rest. It was also assumed that the flow was only from the lower layer. Momentum equation which was applied both infront and behind the skimmer wall had terms and factors to

account for both frictional forces and the non-uniformity of velocity profiles respectively. The force exerted on the skimmer wall was however not considered in the momentum equation. This makes the equation false. In an attempt to account for the energy losses, energy equation was invoked between the two points (upstream and downstream of the skimmer wall) and the frictional force was computed using a drag force relation whereas the non-uniformity of the velocity profiles were corrected by using chosen factors.

The use of skimmer walls for supercritical withdrawal from two-layered fluid system based on incipient conditions was outlined by Jirka (1979). Hydrostatic conditions were assumed for points infront and behind the wall and using one-dimensional energy equation between the selected points, the dynamic head deficit which represents the pressure gradient between the two points was evaluated. The effects of non-uniformity of velocity and head loss were incorporated into the equation.

Dalziel & Lane-Serff (1991) made a contribution in two-layer flows by applying the idea to exchange of warm and cold air through doorways and windows. Their paper outlined the hydraulic description of exchange flows and demonstrated that the basic features of such flows can be described as two-layer flow in a channel with a sharp contraction in height and width. The rule of having a gradually varying streamline (see Armi 1986; Lawrence 1993) as used in internal hydraulic theory was violated in their study.

Adams & Cosler (1988) conducted both theoretical and experimental study of exchange flows using a vertical slotted curtain separating two fluids of different densities. They recognized the fact that at the slotted inlet, the flow is critical and therefore the combined densimetric Froude number should be unity. However their experimental

values of the densimetric Froude number was significantly less than unity. Moreover their definition of the densimetric Froude number which was computed for the experimental values were misleading because the individual layer thickness was not considered for all the cases when there was significant exchange of the two fluids.

Experimentally determined magnitude of the composite Froude number for two-layer flows (both uni-directional and exchange) under sudden obstructions do not have extensive literature but rather is based on the crude measurement of flow rate and the gate opening. Different values of composite Froude numbers have therefore been obtained for cases with and without barotropic forcing. Whiles two-layer flows without barotropic forcing over a sudden obstruction have a unique value (Dalziel & Lane-Serff, 1991), experimental studies (Adams & Cosler 1988; Pawlak & Armi 1997; Harleman & Elder 1958; Rajaratnam & Johnston (Report)) involving two-layers with barotropic forcing or a net flow have different range of values of composite Froude number which makes the characterization very confusing.

Chapter 3

EQUATION DERIVATIONS

3.1 Derivation of Internal Hydraulics

In the following derivation for two-layer flow over a topography, we will consider a smooth sill. The present study considers the steady, two-layer exchange flow of an incompressible fluid over a smooth sill in a horizontal channel of constant width. The flows are assumed to be irrotational, inviscid and the sill is gentle such that hydrostatic pressure can be invoked. The flow is layered and that within each layer, the density is constant and the velocity varies only in the flow direction.

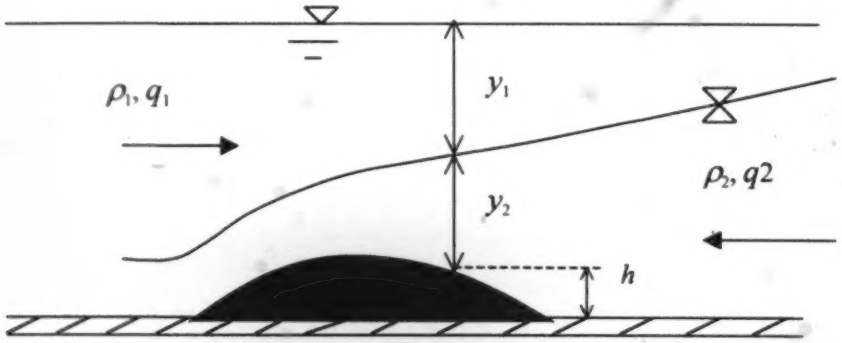

Figure 3.1 Two-layer flow over a smooth sill

With reference to ***figure 3.1***, where h is height of the sill, S represents the surface elevation and y_1, y_2 are depths of the upper and lower layers respectively, the mechanical energy for both layers can be written as:

$$E_i = P_i^* + \frac{1}{2}\rho_i U_i^2 \tag{3.1}$$

where P_i^*, ρ_i and U_i^2 are the piezometric pressure, density and the horizontal velocity respectively. Subscripts $i = 1,2$ represents the upper and the lower layers respectively.

The piezometric pressure can also be expressed as:

$$P_1^* = \rho_1 g(y_1 + y_2 + h) \tag{3.2}$$

$$P_2^* = \rho_1 g\, y_1 + \rho_2 g(y_2 + h) \tag{3.3}$$

where g is the gravitational acceleration. Thus we have

$$E_1 = \rho_1 g(y_1 + y_2 + h) + \frac{1}{2}\rho_1 U_1^2 \tag{3.4}$$

$$E_2 = \rho_1 g\, y_1 + \rho_2 g(y_2 + h) + \frac{1}{2}\rho_2 U_2^2 \tag{3.5}$$

Defining internal energy E as

$$E = \frac{E_2 - E_1}{(\rho_2 - \rho_1)g} \tag{3.6}$$

we can substitute eqns. (3.4) and (3.5) into (3.6) to obtain

$$E = y_2 + h + \frac{1}{2g'}(U_2^2 - rU_1^2) \tag{3.7}$$

where, $g' = (1-r)g$ called the reduced gravity and $r = \rho_1/\rho_2$

For small density difference Boussinesq's approximation can be invoked which means that the effect of density difference can be neglected except in the g' term.

For inviscid and irrotational flow, conservation of energy in both layers in the absence of internal hydraulic jumps means

$$\frac{dE}{dx} = 0$$

where x is the horizontal distance along the channel

That is; $$\frac{d y_2}{dx} + \frac{dh}{dx} + \frac{1}{g'}\left[\frac{d}{dx}\left(\tfrac{1}{2}U_2^2\right) - \frac{d}{dx}\left(\tfrac{1}{2}U_1^2\right)\right] = 0 \qquad (3.8)$$

Now $$\frac{d}{dx}\left(\frac{1}{2}U_1^2\right) = -g' F_1^2 \frac{d y_1}{dx} \qquad (3.9)$$

$$\frac{d}{dx}\left(\frac{1}{2}U_2^2\right) = -g' F_2^2 \frac{d y_2}{dx} \qquad (3.10)$$

where $F_i^2 = \dfrac{q_i^2}{g' y_i^3}$ is the densimetric Froude number, q_i is the flow rate per unit width in the respective layers.

Substituting Eqns. (3.9) and (3.10) into (3.8) yields:

$$\frac{dy_1}{dx} F_1^2 + \frac{d y_2}{dx}\left(1 - F_2^2\right) + \frac{dh}{dx} = 0 \qquad (3.11)$$

With Boussinesq's approximation we have a horizontal free surface, thus

$$\frac{d y_1}{dx} + \frac{d y_2}{dx} + \frac{dh}{dx} = 0 \qquad (3.12)$$

Substitution of Eqn. (3.11) into (3.12) we then write the slope of the interface as

$$\frac{dy}{dx} = -\frac{F_2^2 \dfrac{dh}{dx}}{1 - \left(F_1^2 + F_2^2\right)} \qquad (3.13)$$

where the interface position $y = y_2 + h$

Introducing topographic slope $S_o = F_2^2 \dfrac{dh}{dx}$, eqn.(3.13) can be written as:

$$\frac{dy}{dx} = -\frac{S_o}{1-G^2} \tag{3.14}$$

where $G^2 = F_1^2 + F_2^2$ is called the composite or internal Froude number.

From eqn.(3.14) it could be deduced that at the point of maximum sill height $\frac{dh}{dx} = 0$. Since the flow is accelerating, the interface slope $\frac{dy}{dx}$ is not zero so for the flow to be critical G^2 should be equal to unity (G^2=1). The other condition for critical flow will occur in a region outside the topography for which $\frac{dh}{dx} \neq 0$, but G^2=1. In order that $\frac{dh}{dx}$ be finite at this section, $F_2^2 \approx 0$ for which case $F_1^2 \approx 1$. It should be noted that this is not necessary the case. For instance in the experimental study by Zhu (1996) the second control was found to be at the rectangular channel exit due to the expansion of the channel width. This point is called the exit control. For two-layer flow over a smooth sill there are three regimes of flow, namely unsteady regime, followed by maximal and finally the submaximal. The maximal regime is the only regime where the flow has two controls and it is the steady state. The second control in most experimental studies on internal hydraulics vary according to the flow regime. Eqn.(3.14) has been extended by Zhu & Lawrence (1996) for cases where effects of friction and non-hydrostatic forces due to streamline curvature are important. Their extended equation is as below:

$$\frac{dy}{dx} = \frac{S_f - S_0 - S_c}{1-G^2} \tag{3.15}$$

where S_f is the friction slope and Sc is the energy slope owing to streamline curvature. It can also be seen from eqn.(3.15) that at the point of maximum sill height, the

numerator is not zero which means that the control point is at a different location when factors other than the topographic slope are considered.

3.2 Prediction of Flow Rate

The internal hydraulic theory as derived in ***section 3.1*** for non-barotropic forcing of two-layer flow over a smooth sill can be applied to flows through openings. With reference to ***figure 3.2***, a diagram which is similar to ***figure 3.1*** has been sketched for two-layer flow through an opening. The dotted line in the diagram represents an ineffective flow area. This will be explained in detail for flows without forcing in §5. This region in fact represents the vortex formation around the opening in the less dense fluid and by virtue of it shape, it acts as a sill for the upper layer. Beyond the opening towards the left, there is a region of discontinuity as a result of submerged internal hydraulic jump.

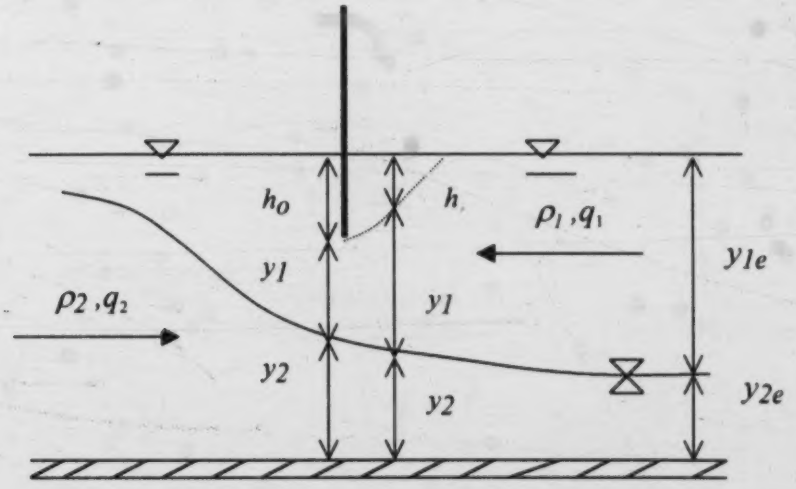

Figure 3.2 Exchange flow through an opening

Equation (3.16) below is the internal energy, which was obtained by considering the fact that the opening acts as an inverted sharp sill which is basically not different from the smooth sill.

$$E = y_2 + \frac{1}{2g'}(U_2^2 - U_1^2) \tag{3.16}$$

For maximal exchange flows there exists two hydraulic controls. The first control is at the point of maximum topography (the gate); the other control is at the exit.

Condition 1:

At the point of maximum the topography Composite Froude number $G^2 = 1$

$$\Rightarrow \quad \frac{U_{1o}^2}{g\, y_{1o}} + \frac{U_{2o}^2}{g\, y_{2o}} = 1 \tag{3.17}$$

Condition 2:

At the exit control $G^2 = 1$ for $\frac{dh}{dx} \neq 0$ (singularity condition)

$$\Rightarrow \quad \frac{U_{2e}^2}{g\, y_{2e}} + \frac{U_{1e}^2}{g\, y_{1e}} = 1 \tag{3.18}$$

Condition 3

Continuity equation for the upper layer means

$$U_{1o} y_{1o} = U_{1e} y_{1e} \tag{3.19}$$

Condition 4

Continuity equation for the lower layer means

$$U_{2o} y_{2o} = U_{2e} y_{2e} \tag{3.20}$$

Condition 5

Conservation of energy means internal energy at the maximum topography (gate) and the exit control should be the same

$E_O = E_e$

$$\Rightarrow \quad y_{2o} + \frac{1}{2g}(U_{2o}^2 - U_{1o}^2) = y_{2e} + \frac{1}{2g}(U_{2e}^2 - U_{1e}^2) \tag{3.21}$$

Conditions 6

Definition of water depth at the point of maximum topography (gate) means

$$y_{1o} + y_{2o} = H - h_o \tag{3.22}$$

Condition 7

Definition of total depth at the exit control means

$$y_{1e} + y_{2e} = H \tag{3.25}$$

Condition 8

At steady state flows in both layers are the same

$q_1 = q_2$

$$\Rightarrow \quad U_{1o} y_{1o} = U_{2o} y_{2o} \tag{3.26}$$

These non-linear equations were successfully solved using MATLAB® and it has been applied to predict the flow rate for non-barotropic forcing experiments which will be discussed later in chapter 5. It should be noted that this prediction is for inviscid and irrotational flow where non-hydrostatic forces can be neglected.

Chapter 4

EXPERIMENTAL APPARATUS AND TECHNIQUES

The experimental study to investigate the mechanism of control for two-layer flow through an opening adopted a planar sluice gate. This gate was located in a long rectangular channel separating two reservoirs containing fresh and salt water. The experiments were conducted for cases involving both barotropic and non-barotropic forcing.

4.1 Experimental Design and Set-up

For steady two-layer flows, the volumetric flow rate per unit width of the channel $q = Q/b$ depends on: the size of the opening (d), the total water depth in the channel (H), the channel length (L) and the width (b), the density of the fluid for both layers (ρ_1 and ρ_2), the gravitational acceleration (g), viscosity (μ) and the head difference (ΔH) for the cases with barotropic forcing:

$$q = f(d, H, L, b, \rho_1, \rho_2, g, \mu, \Delta H) \qquad 4.1$$

The effects of temperature have not been explicitly included, however it is accounted for by incorporating the densities. Also for Boussinesq's type of flow, the gravitational acceleration could be replaced by the reduced gravity g' which is defined as $g' = (\rho_2 - \rho_1)/\rho_2 \times g$. Dimensional analysis carried out on Eqn. (4.1) for the repeating variables of ρ_2, g' and H yielded the following results:

$$q/\sqrt{g' H^3} = \varphi(d/H, L/H, b/H, \Delta H/H, \rho\sqrt{g' H^3}/\mu) \qquad 4.2$$

The term $\rho\sqrt{g' H^3}/\mu$ represents the characteristics Reynolds number. The number of variables in Eqn. (4.2) can be reduced if the total water depth H, the length of the channel L and the channel width b are fixed in the experiments for the case of non-barotropic forcing. This leaves three parameters; d, g' and Re, which can be varied to study the flows under the various experimental conditions. The effects of the variation of ΔH was studied by pumping water from one reservoir to the other. This resulted in a net flow and it was used to study the mechanism of control through the opening for barotropic forcing.

In the present study for the case involving non-barotropic forcing, attention was focused on the effects of opening d and experiments were conducted mainly by varying d. The Reynolds number is implicitly varied because a variation in d will vary the flow velocity in both layers resulting in the variation of the Reynolds number.

The experiments were conducted in a large tank made of plexiglass and of dimensions 243*cm* x 122.5*cm* x 35*cm* as shown in ***figure 4.1***. This large tank was partitioned at mid-length to accommodate both fluids on either side. A rectangular channel having a length of 150*cm* and width of 10*cm* connected the two tanks. A sluice gate was created at approximately 60cm from the tank containing the denser fluid to form an opening as shown in ***figure 4.1***

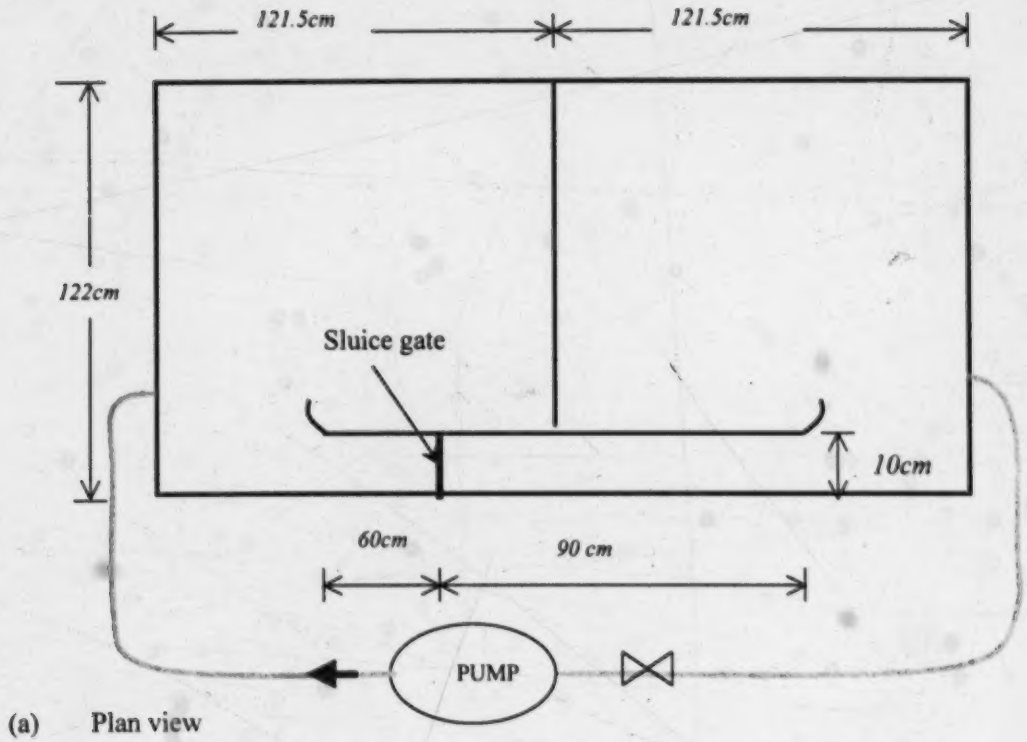

(a) Plan view

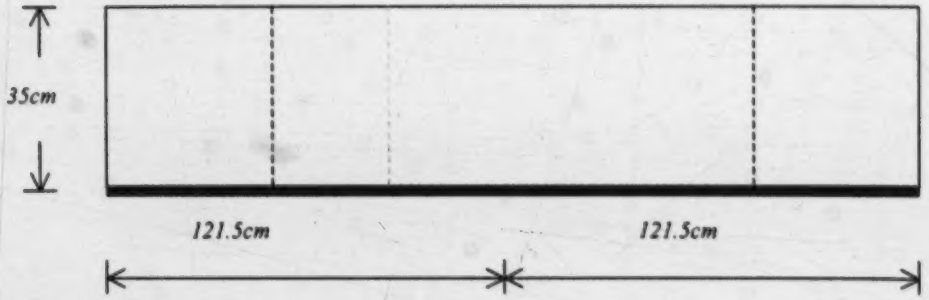

(b) Side view

Figure 4.1: Plan and side view of the experimental set-up

Three series of experiments were carried out. In all the experiments, 1700 *grams* of salt (Windsor brand manufactured by The Canadian Salt Company Limited) was used. The first series of experiments were conducted for non-barotropic forcing at different sluice gate openings (d ~ 8 - 22 *cm*). This was followed by barotropic forcing experiments in which the same channel dimensions as in the non-barotropic forcing was used. Gate openings (d) in the range of 8 – 22 *cm* were investigated. The experimental studies conducted for the case involving barotropic forcing had a net flow, which was created by pumping the salt water from the bottom of the fresh water reservoir back to the salt water reservoir. A pump with maximum a capacity of 238 cm^3/s (model 3-MD-SC manufactured by Little Giant Pump Company, Oklahoma City) was used. The pump was started after sufficient amount of time has elapsed after the gate opening to make sure that the water pumped back was indeed salt water. This left the exit control in a subcritical state.

The last set of experiment was therefore conducted for the same barotropic forcing but this time the bed of the original rectangular channel connecting the two reservoirs was raised by 7.5 *cm*. The idea of raising the channel bottom was to allow an earlier start-time of the pump so as to avoid an early submergence of the exit control. The momentum of the pumped water was damped using a sponge as an energy dissipator. ***Tables 4.1, 4.2*** and ***4.3*** show complete lists of all the different experiments.

Experiment #	Gate opening d (cm)	Depth of water H (cm)	Temp. (°C)	Reduced gravity g' (cm/s^2)	Flowrate at steady state q (cm^2/s)	Predicted flowrate q (cm^2/s)	Re=q/ν
1	22.0	30.0	19.5	2.74	36.80	36.92	3871
2	19.0	30.0	18.5	2.74	27.41	28.15	2779
3	17.0	30.0	22.0	2.72	25.72	24.42	2712
4	14.0	30.0	19.5	2.74	18.94	18.00	1925
5	11.0	30.0	21.5	2.73	14.42	12.63	1479
6	8.0	30.0	18.5	2.74	8.19	7.81	859

Table 4.1 Non-barotropic experiments

Experiment #	Gate opening d(cm)	Depth of water H (cm)	Temp. (°C)	Reduced gravity g' (cm/s^2)	Flowrate in upper layer q_1 (cm^2/s)	Flowrate in lower layer q_2 (cm^2/s)	Net Flowrate q_2-q_1 (cm^2/s)
7	22.0	30.0	22.0	2.72	5.14	31.91	26.77
8	14.0	30.0	21.5	2.73	0.96	27.57	26.61
9	10.0	30.0	20.5	2.73	0.88	27.19	26.31

Table 4.2: Barotropic forcing experiments without exit control

Experiment #	Gate opening d(cm)	Depth of water H (cm)	Temp. (°C)	Reduced gravity g' (cm/s^2)	Flowrate in upper layer q_1 (cm^2/s)	Flowrate in lower layer q_2 (cm^2/s)	Net Flowrate q_2-q_1 (cm^2/s)
10	14.5	22.5	22.5	2.72	6.94	28.31	21.37
11	10.5	22.5	22.5	2.72	2.04	23.46	21.42
12	7.5	22.5	22.5	2.72	1.68	23.51	21.83
13$^{\psi}$	14.5	22.5	12.0	2.84	8.68	29.24	20.56

ψ: *this experiment had the elevated channel bed extended to the end of the reservoir.*

Table 4.3: Barotropic forcing experiments with elevated channel bed

4.2 Experimental Preparation

Both reservoirs were initially filled with water to the same level before the gate was closed. The temperature of the water was recorded. 1700 grams of salt was dissolved in the salt water reservoir. The densities were computed with the highest accuracy in the order of 3 decimal places using interpolated values from experimental measurements compiled by Lide (1998) as shown in ***figure 4.2***. Pliolite particles were added and mixed into both reservoirs. This was followed by the addition of Sodium Fluorescein dye into the salt water reservoir. The water was stirred for several minutes to ensure that the contents were uniformly distributed. The experiments were performed in a dark room. The flow in the channel was illuminated using a sheet of light generated by two 500-Watt Halogen bulbs.

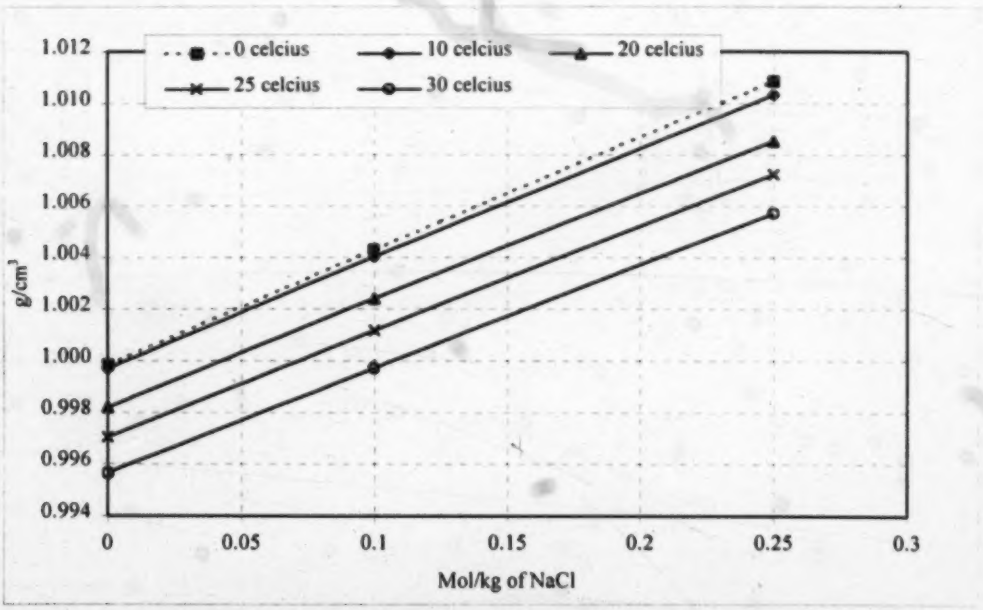

Figure 4.2 Salt water(NaCl) density estimation from the weight concentration of NaCl. Symbols are the experimental values by Lide (1998).

The objective of the experimental study demanded that both the interface positions and the flow rate be measured simultaneously. Two video cameras were therefore required for the study. The recording facilities were set up and physical scales were recorded to calibrate video images. Having achieved quiescent conditions in both reservoirs, the experiments were started by adjusting the sluice gate to the desired opening.

4.3 Velocity and Interface Position Measurements

Velocity measurements were obtained by mixing tiny buoyant particles into both fresh and salt water reservoirs and then recording their movements. Pliolite VT-L particles (Manufactured by Goodyear Tire & Rubber Company) which is insoluble in water, possesses high degree of reflectivity and a density of 1.026 g/cm^3 was adopted for the experimental study. Particles of sizes in the range of 0.208μm to 0.400 μm were mixed in a small amount of detergent and then added to both tanks. Both tanks were stirred thoroughly to achieve a homogeneous distribution of the particles. The idea of mixing the Pliolite particles in small amount of detergent is to break the surface tension. The particle settling velocity estimated by Zhu (1996) shows that the values are insignificant to distort the velocity measurements. Physical scales made of $5cm \times 5cm$ square grids was used for the calibration of recorded images for both the flow rate and interface positions.

Particle movement was recorded using a *Sony digital-8* digital camera (with lens 1:1.4/36-72mm) which was focused close to the plexiglass at a region free from rotation (x/L~0.5-0.9). The particle sizes in the recorded video images were in the range of 1-3 pixels. The recorded images were captured by a Pentuim III computer using the ATI

frame grabber board for windows 95 followed by another software MEDIA STUDIO version 2.5. The images were grabbed at a rate of 5 frames per second. Two images taken at different times formed a pair. The captured images which had 640x480 pixels in size were saved as TIFF files and further analyzed using PV-Wave (by Visual Numerics Inc.).

Maximized cross-correlation technique for resolving velocity fields (Stevens & Coates, 1994) was applied between successive images to obtain the velocity field. This technique assumes that changes in the intensity distribution due to straining or rotation are small compared to translation. A grid of nodes, at which velocities are required, is set up on the first image. A window of certain size is extracted, centered on each node in turn. The second image is then searched for a similar window of the same size that is maximally spatially correlated to the first window. With these a set of displacement vectors regularly spaced over the image describing "instantaneous" velocity field can be obtained. Post-processing of the data using multi-pass filter to removes the erroneous vectors. Since a shortcoming of this maximized cross-correlation technique is its inability to analyze flows with straining and rotation, the time interval and the window size were chosen such that the effects of non-translational motion can be reduced to the barest minimum. Velocity field was computed from 4 pairs of images and then averaged to give a more reliable result.

The interface between the two layers was visualized by adding Soduim Fluoroscein dye to the lower layer. This dye has light reflective property that makes the visualization of the interface positions very easy once the experiment is in progress. The interface positions were also recorded using another *Sony Hi-8* camera (with lens 1:1.8/5.5-54*mm*). The camera for the interface position measurement was focused on the whole

experimental region. The measurement of flow rate in the lower layer was also not a problem once a smaller amount of dye has been used; this allows a distinct location of the interface as well as the of the clear visualization of the particles in the lower layer. The interface positions were taken at every 15 seconds and then averaged for each minute. The choice of 15 seconds was considered appropriate because the interface positions were fairly constant at the steady state flow regime. The averaging of the interface positions was necessary because of interfacial instabilities. The interface positions were measured with software called SCION IMAGE. This software is used to determine the location of the interface position in pixels based on visual observation. This helped in eliminating errors associated with interface location such as the influence of entrainment and interfacial mixing. Although average values of interface positions were used, the presence of interfacial instabilities can cause a slight deviation. For given successive images typical of this experimental study where the reduced gravity g' was in the range of 2.72-2.74 cm/s^2, the interface deviation due to instabilities were of the order of 0-3mm from the mean.

For a given camera image, the extreme edges appear to be farther than the central region. This makes the physical scales slightly different for a frame taken at the same time. The variation is usually in the order of 1 to 3 pixels. The flow rate calculation therefore considered the average of scales from three different locations along a frame. For the interface computation, the vertical scale was calculated for each pixel along the channel; this corrected the variation of the vertical scale. The horizontal scale was also calibrated by choosing points along the entire test region.

Chapter 5

EXPERIMENTAL RESULTS AND DISCUSSIONS

On the whole three sets of experiments were carried out. The first series were for the case of non-barotropic forcing. The second series considered the influence of barotropic forcing by creating a net flow between the upper and the lower layers using a pump for the same channel dimensions in the first experiment. The last set of experiment was also for barotropic forcing but the original rectangular channel bed was raised by 7.5cm.

5.1 Non-barotropic Experiments

Table 4.1 gives a list of the non-barotropic experiments with experimental conditions such as temperature, reduced gravity and gate opening. The measured flow rate is also given, together with the Reynolds number, $Re=q/\nu$.

5.1.1 Evolution of the Flow

The experiments conducted for the non-barotropic forcing had the mean flow evolved through three regimes after the experiments were started by opening the sluice gate. The regimes were classified into three: namely, unsteady, maximal and submaximal (see Zhu & Lawrence,1999).

The unsteady regimes started right after the gate removal. Gravity currents developed and gradually an unsteady exchange flow was established. Photograph illustrating this regime can be found in ***figure 5.1(a)***. During this start-up period, slight mixing occurred but the mixed fluid was gradually advected into the supply reservoirs.

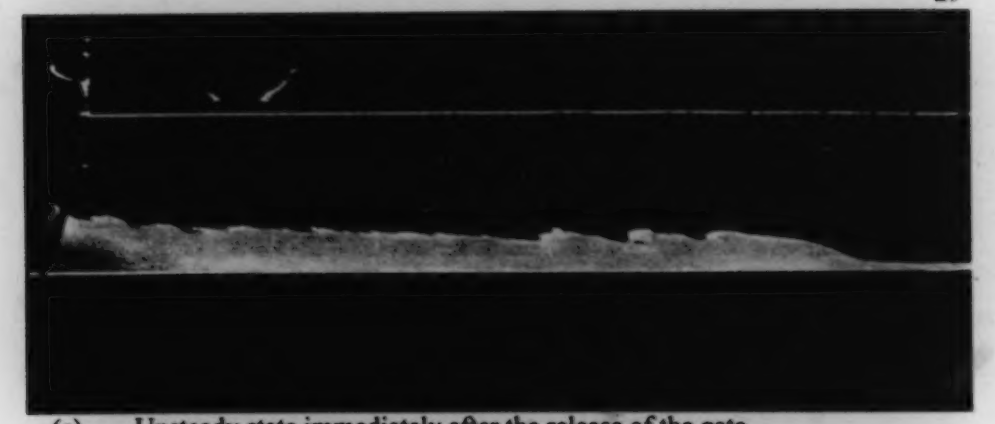

(a) Unsteady state immediately after the release of the gate.

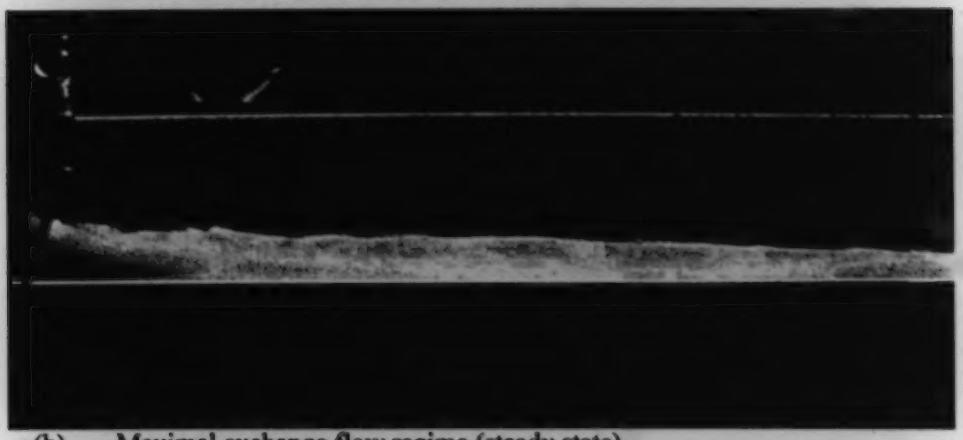

(b) Maximal exchange flow regime (steady state).

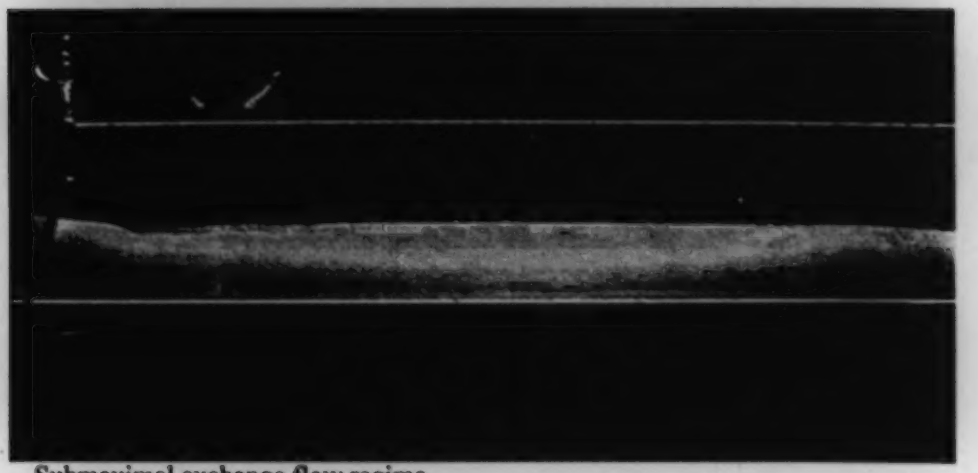

(c) Submaximal exchange flow regime .

Figure 5.1 Regimes of exchange flow without barotropic forcing.

This period is unsteady and for that reason values of both flow rate and interface positions were not used in the analysis. The hydraulic control at the gate was established first, and the exit control was established at a later time.

The maximal flow regime is considered to be the period of steady state. There are two hydraulic controls for this type of flow; one at the gate and the other at the exit of the channel. In between the controls, the flow remained subcritical with a constant flow rate and interface position. ***Figure 5.1(b)*** is a photograph of maximal exchange flow regime.

The last regime which is called submaximal ocurred when the exit was submerged due to the rise in the level of he interface in the right hand reservoir. This submaximal exchange regime had only one hydraulic control (at the gate) and a smaller flow rate. Photograph illustrating this regime can be found in ***figure 5.1(c)***. As the experiments proceeded, the interface level at the gate gradually decreased, while that at the exit gradually increased.

5.1.2 Measurements of Flow Rate and Interface Positions

Measurements of flow rate and interface positions were carried out simultaneously as described in §4. In arriving at the average flow rate to represent any given experiment for non-barotropic forcing, the flow rate curves were classified into three regimes; unsteady, maximal and submaximal flow regimes as already discussed in ***section 5.1.1***. These regimes for a typical flow rate curve which was obtained from experiment #3 has been shown in ***figure 5.2***.

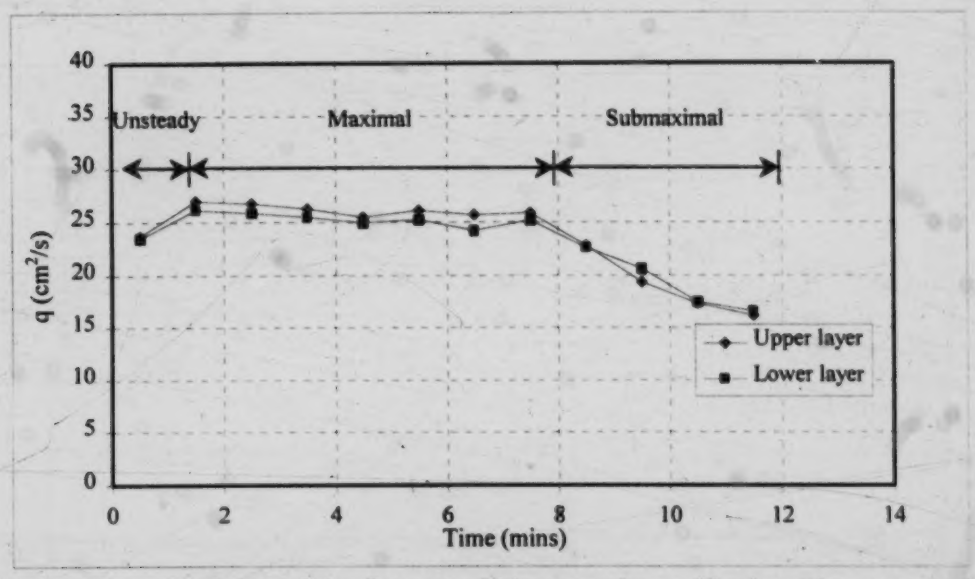

Figure 5.2 Variation of the flow rate during experiment #3 where the gate opening $d=17cm$ and $H=30cm$.

The initial points starting the curve were not considered because those points represent unsteady state after the release of the gate. The average flow rate was computed at steady state ($q_1 = q_2$). This was arrived at by averaging the flow rate for the upper layer computed at points within the fairly horizontal section of the flow rate curve. This fairly horizontal section is in fact the maximal exchange flow regime which represents the steady state. The flow rate curve for the submaximal regime indicates a reduction in the flow rate values for both layers. Based on maximal exchange flow conditions already presented in §3, the flow rates for the non-barotropic experiments were predicted using these non-linear equations (eqns. 3.17 to 3.26) with the aid of MATLAB®. The results together with the measured flow rate at steady state have been plotted in ***figure 5.3***. The flow rate is well predicted with a percentage deviation of ± 0.3-11%.

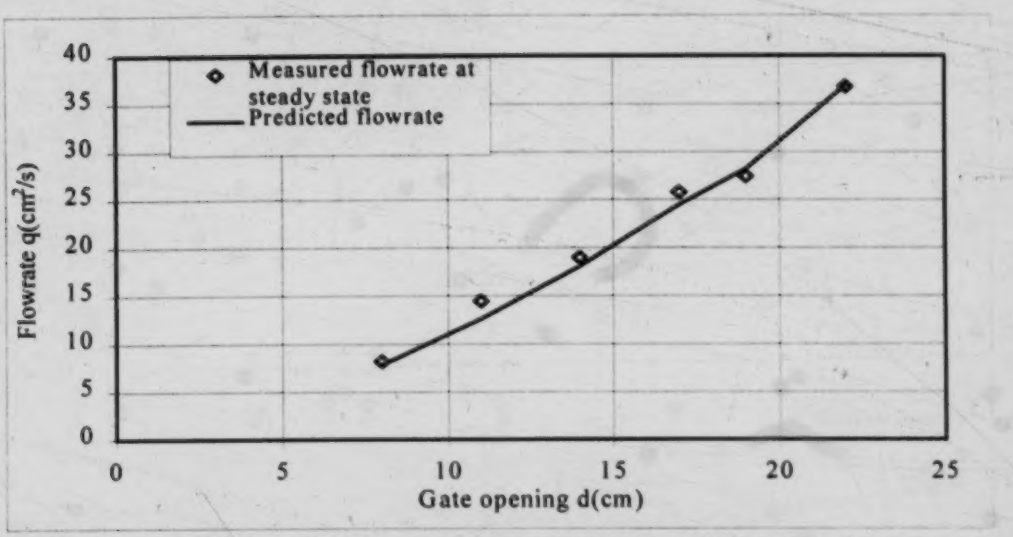

Figure 5.3 Comparison of flow rates for the non-barotropic forcing experiments

The streak path of the pliolite particles in the upper layer, which represents the flow pattern at the upstream side of the gate was very difficult to follow for each set of experiment. The reason is that, their path is dependent on the gate opening, duration (time) and density difference which is also a function of temperature. Direct measurement of streak photograph for each experiment was not carried out, instead, streak photographs were taken for few trial experiments. The upper layer converges when it passes under the gate and the formation of a circulating eddy upstream of the gate as shown in ***figure 5.4*** depicts the pattern of flow. This figure is a streak photograph taken with an exposure time of ¼ of a second using ISO 400/21 film. This circulating eddy effectively reduces the thickness of the upper layer. The size of the eddy decreases exponentially to zero at approximately 4 to 5 times the length of the gate submergence away from the gate.

Figure 5.4 Steak photograph taken with exposure time of *¼ of a second* to portray the flow pattern in the upper layer for experiment #2. The gate submergence h_o in this case is 11cm.

The effective eddy region around the gate was estimated as

$$h = h_o e^{-14.3\left(\frac{x}{L}\right)} \tag{5.1}$$

Where: h_o: is the gate submergence (or the height of the sharp sill)

h: is the correction to be deducted from the upper layer at any location x along the rectangular channel

L is the length of the rectangular channel

x: is the horizontal distance along the channel with the origin at the gate.

In effect upper layer thickness y_1 becomes

$$y_1 = (H - y) - h_o e^{-14.3\left(\frac{x}{L}\right)} \tag{5.2}$$

where y is the interface position.

This logarithmic curve was based on trial fit curves for streak photographs and can only be applied to the non-barotropic experiments. It must also be pointed out that the determination of the effective flow area was not crucial since the objective of this experimental study was to determine the flow conditions at the gate and the exit. The choice of this curve however gave a fairly good representation of the flow pattern which was helpful in the computation of the composite Froude number along the channel. A sample of graph representing the variation of the interface profile together with the correction for the upper layer along the channel is shown in ***figure 5.5***. Measurement of flow rate and interface positions for experiments #1 to #6 are presented in the ***Appendix***.

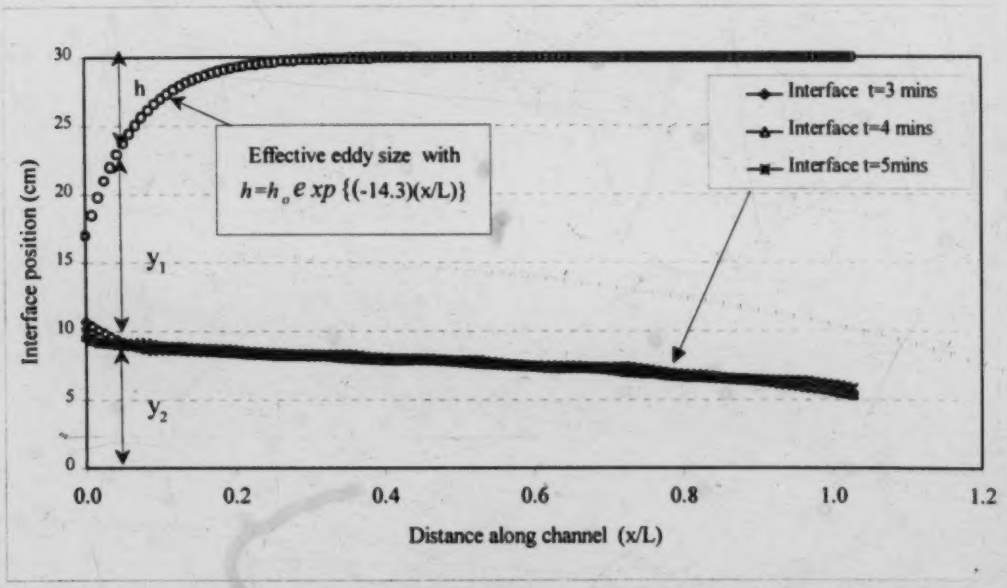

Figure 5.5: The variation of average interface positions with time from the gate to the channel exit for experiment #3 with gate opening *d=17cm* and *H=30cm.*

Figure 5.6 shows a plot of the averaged interface positions at the gate and the channel exit at consecutive times during the experiment. It can be observed that at time t = 6 minutes, the interface level at the gate exit begins to rise. This gradual rise in the interface level at the channel exit ultimately leads the steady state (maximal regime) to the submaximal regime where the exit no longer becomes as hydraulic control.

The variation of internal energy at steady state (t=3minutes) for experiment #3 can be found in ***figure 5.7***. While the inviscid and hydrostatic theory would predict a constant internal energy, this curve indicates the that internal energy is not constant. This is due to frictional effects, streamline curvature and the vortex formation infront of the gate. ***Figure 5.8*** is a streak photograph taken to indicate the flows beyond the sluice gate which represents region of discontinuity. There is in fact an inverted hydraulic jump within this region

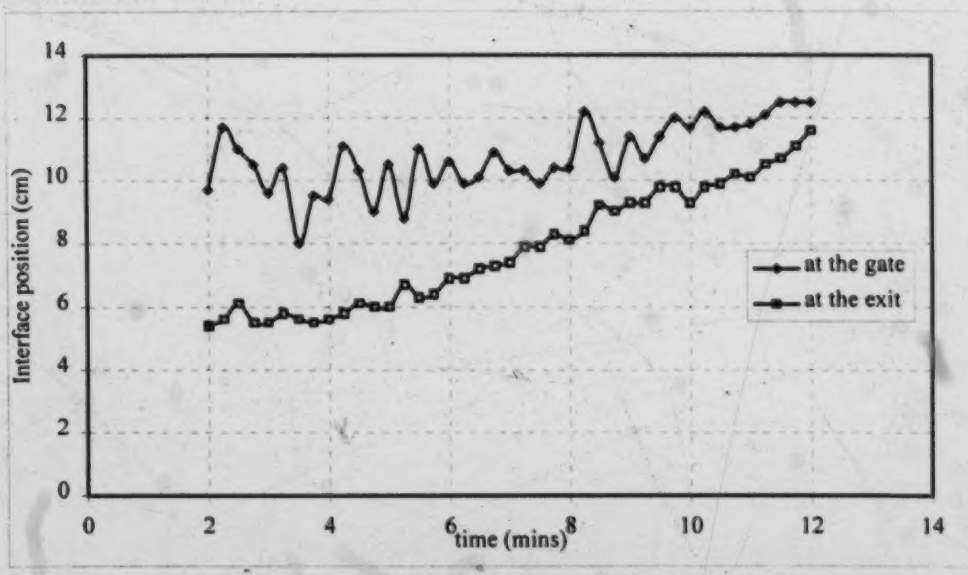

Figure 5.6 Plot of interface positions with time at the gate and the channel exit for experiment #3 which has gate opening *d=17cm* and *H=30cm*.

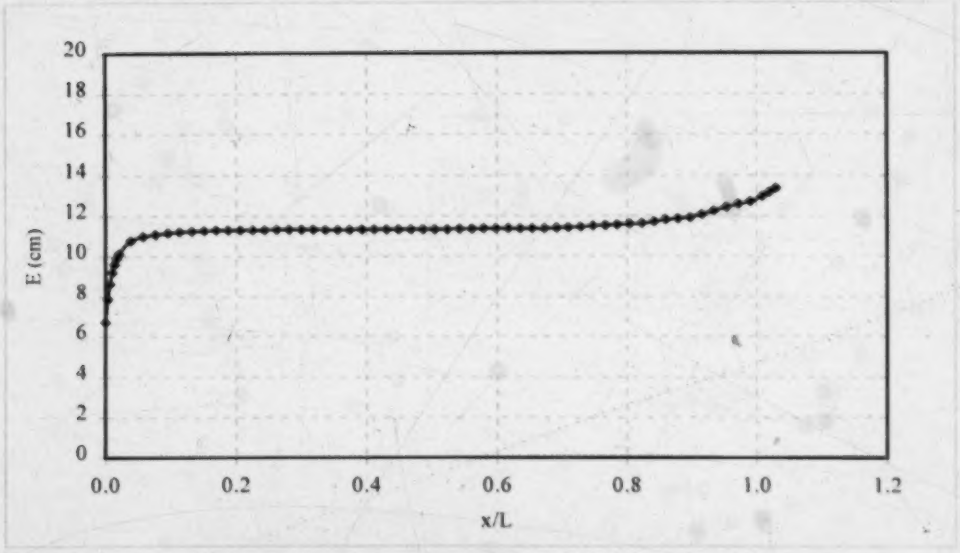

Figure 5.7 Variation of internal energy (E) along the channel at time time *t=3 minutes* in experiment #3.

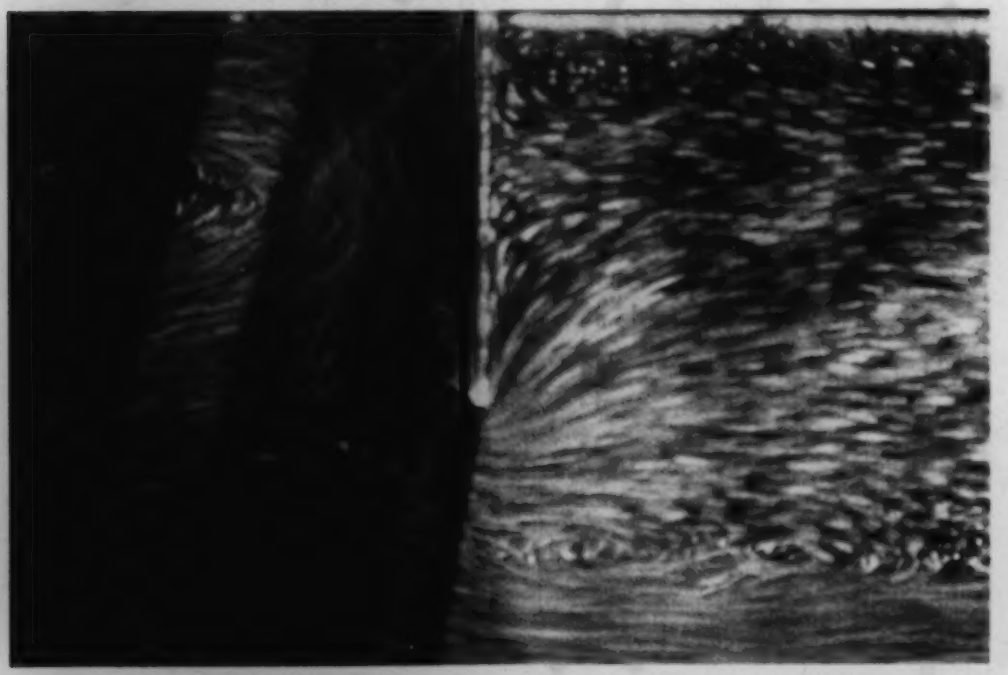

Figure 5.8 Steak photograph taken for an exposure time of *¼ of a second* to portray the flow pattern just beyond the gate.

5.1.3 Composite Froude Number

Plots of composite Froude number for all non-barotropic experiments are presented below. The composite Froude number G is very sensitive close to the gate, thus accurate determination of G at the gate is difficult. All the experiments have $G>1$ at the exit. The exit control shifted within the channel to somewhere between $x/L\approx0.9$-1.0. The variation of the composite Froude number for this set of experiments will be discussed in detail in the ***section 5.3***. ***Figure 5.9(a)*** shows the variation of Froude numbers for the upper and the lower layers for experiment #3.

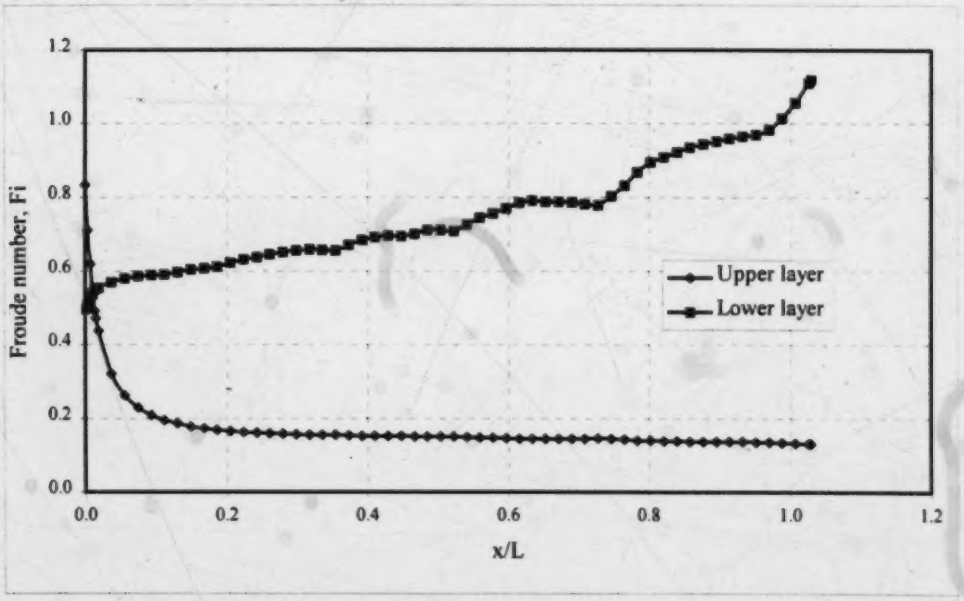

Figure 5.9(a) Froude numbers for the upper and lower layers in experiment #3 at t=5 minutes. Gate opening $d=22cm$ and $H=30cm$.

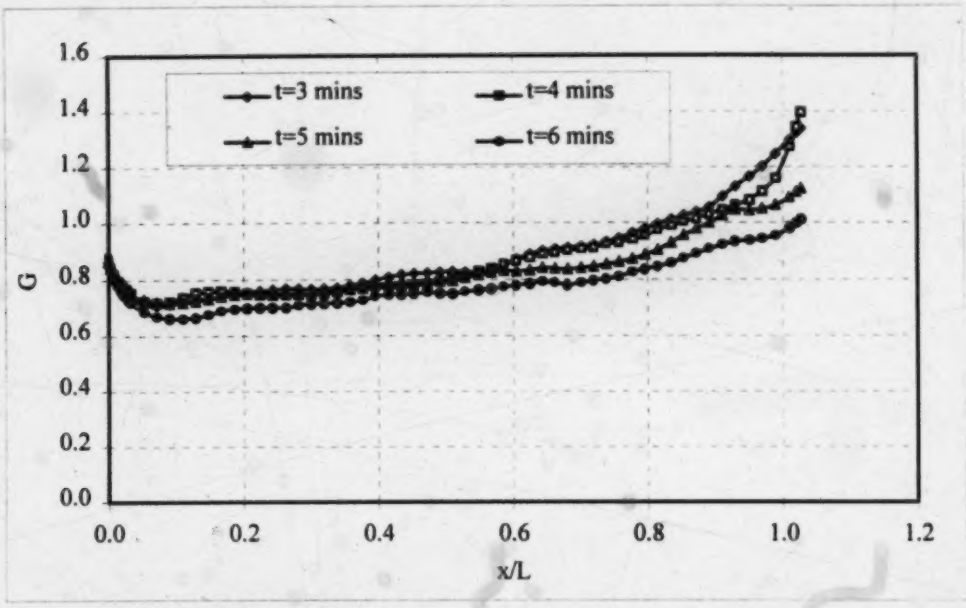

Figure 5.9(b) Composite Froude number G for experiment #1 with gate opening *d=22cm* and *H=30cm*.

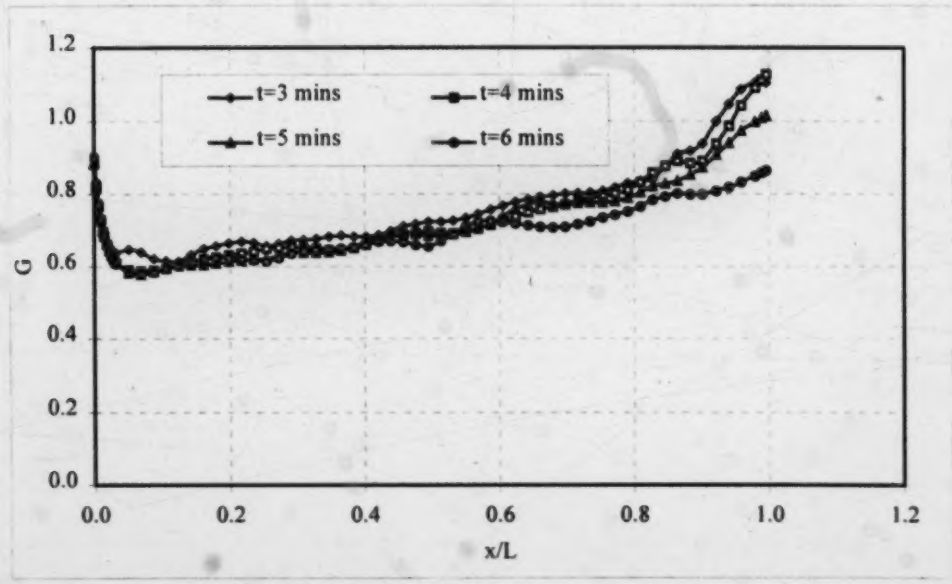

Figure 5.10 Composite Froude number G for experiment #2 with gate opening *d=19cm* and *H=30cm*.

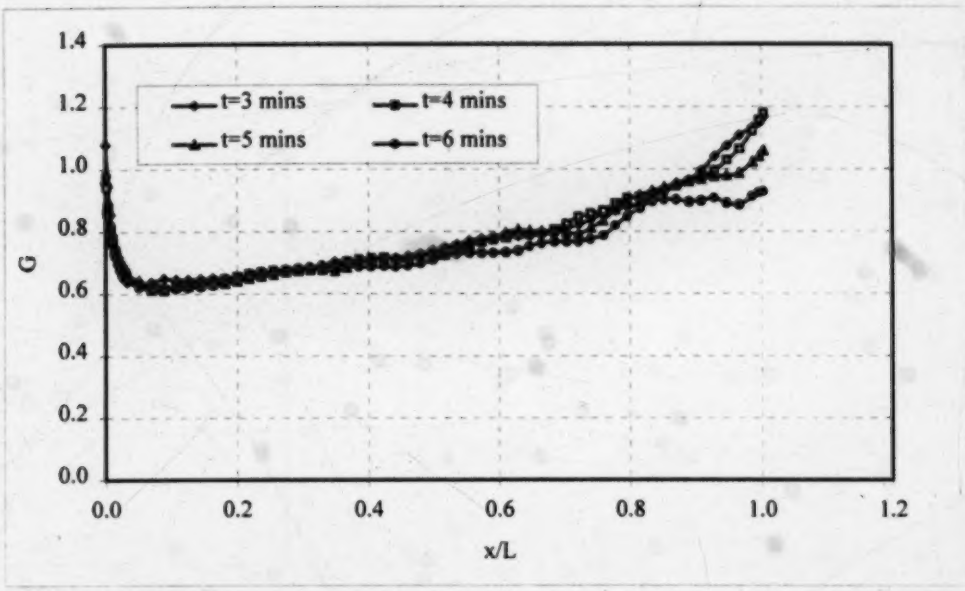

Figure 5.11: Composite Froude number G for experiment #3 with gate opening *d=17cm* and *H=30cm.*

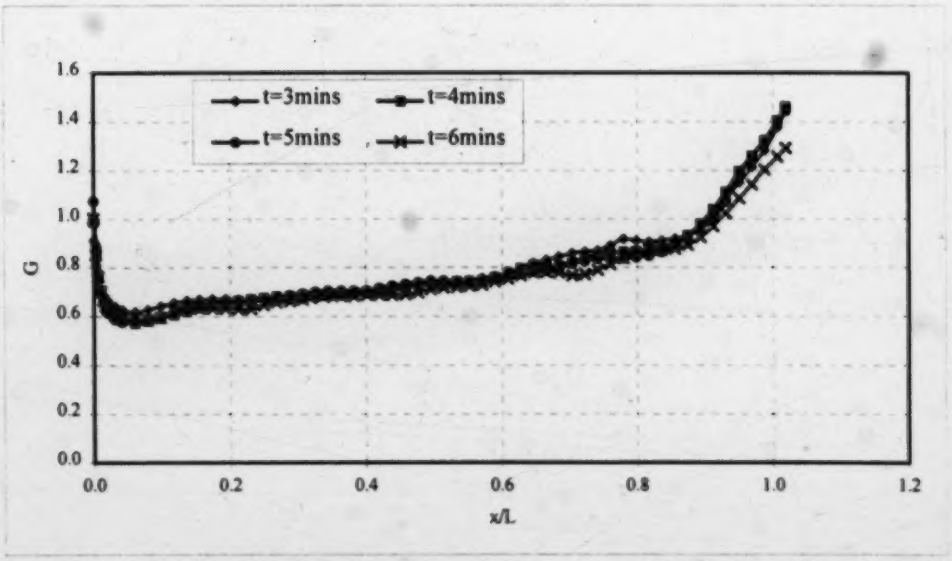

Figure 5.12 Composite Froude number G for experiment #4 with gate opening *d=14cm* and *H=30cm.*

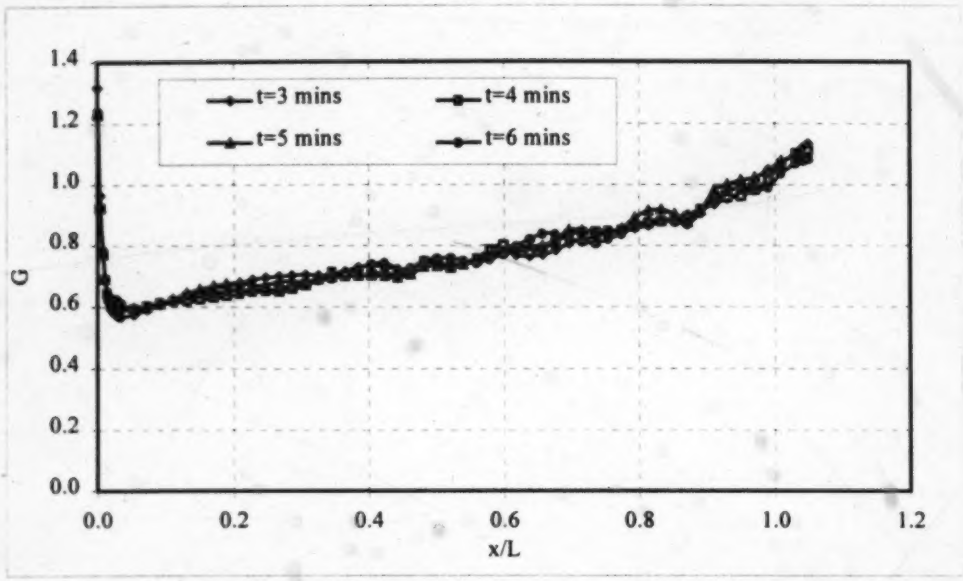

Figure 5.13 Composite Froude number G for experiment #5 with gate opening *d=11cm* and *H=30cm*.

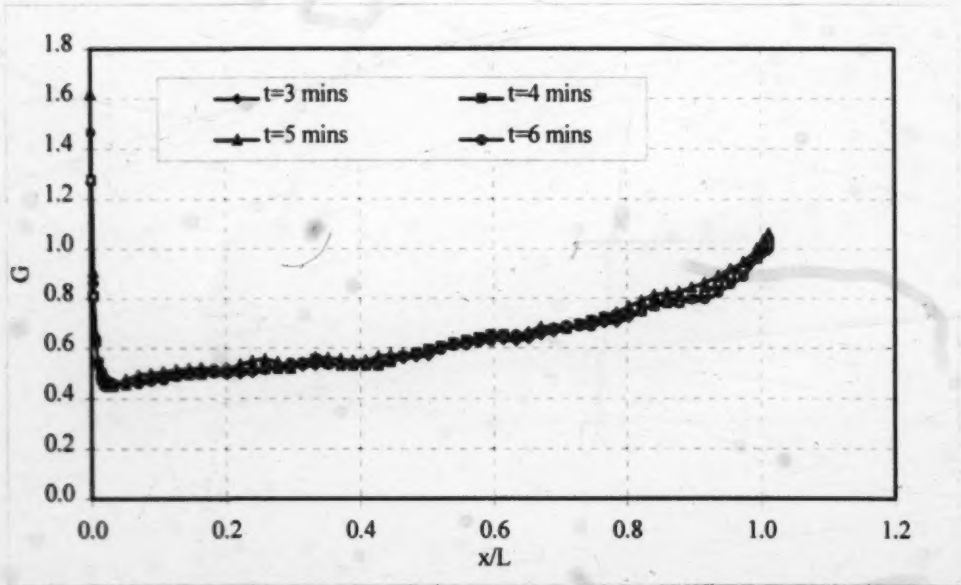

Figure 5.14 Composite Froude number G for experiment #6 with gate opening *d=8cm* and *H=30cm*.

It should be pointed out that time in minutes is not a good parameter to compare all the experiments. This is because the rate of exchange in each experiment varies according to the gate opening and the density difference. The time indicated on each plot however represents steady state measurement. It can be observed that the values of composite Froude number at the channel exit decreases with time which suggests that the exchange flow is in the submaximal regime.

Also as a point of interest for the non-barotropic experiments, the composite Froude numbers were plotted against their gate openings. The plot can be found in ***figure 5.15***. One observation is that, the composite Froude number increases as the opening reduces which suggests that the upper layer accelerates and thins down as it passes the gate making the its Froude number higher. For larger gate openings (higher d/H ratios), the composite Froude number is lower compared to the smaller gate openings. This can be attributed to the fact the smaller gate openings imposes high non-hydrostatic effects which results in higher values of composite Froude number G at the gate.

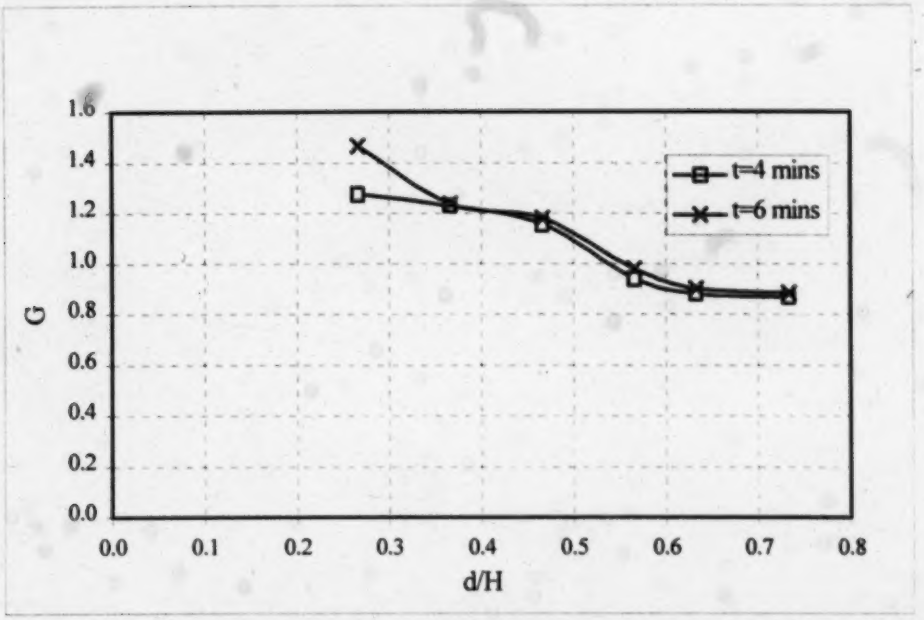

Figure 5.15 Plot of composite Froude number G versus d/H for non-barotropic forcing experiments at times $t = 4$ and 6 minutes

5.2 Barotropic Forcing Experiments Without Exit Control

The barotropic experiments were conducted with and without the elevated channel bed as has been outlined in §4. All the experiments had a net flow, which was created by pumping salt water from the right hand reservoir to the left. The pump was initially primed with salt water to get rid of all the trapped air in the connecting tubes. Visual observation of the interface level in the right hand reservoir after the release of the gate was very important since an earlier start time of the pump can result in the pumping of both fresh water and salt water. The combination of the fresh and salt water at the pump intake can distort the results.

Discussions centered on the first set of experiments on barotropic forcing which is basically the ultilisation of pump to create a net flow between the upper and the lower layers for the same channel dimensions as in the non-barotropic experiments will henceforth be called "barotropic forcing without exit control". The last set of experiments which had the original rectangular channel bed elevated by 7.5cm will also be called "barotropic forcing with exit control".

The pump was switched on at approximately *5* to *8 minutes* after the released of the gate. The duration for the pump start-up was dependent on the rate of exchange flow which was a function of density difference and the gate opening.

In all the experiments, measurements were taken after *3* minutes of the pump start-up. It can be seen that the entire duration of the flow measurement as plotted in ***Figure 5.16*** for experiment #7 is fairly horizontal. This represents steady state and it is in fact the case

as long as the pump is operational. Similar results for the rest of the experiments can also be found in ***Appendix.***

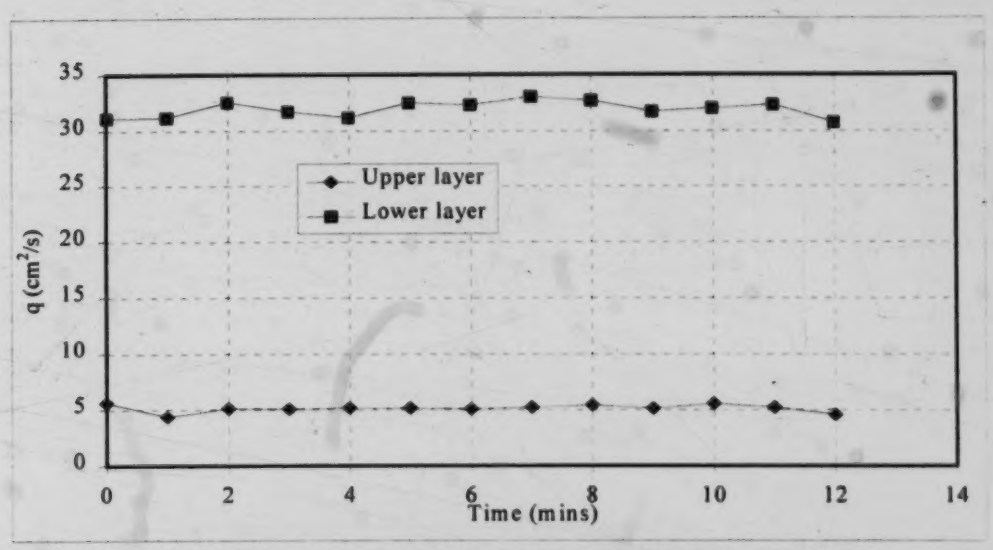

Figure 5.16 Plot of flow rate curve for experiment #7 after 3minutes of the pump start-up. This experiment had gate opening *d=22cm* and *H=30cm*

Correction was not applied to the effective flow surface in the upper layer. This is because in most of the experiments, the flow in the upper layer was very slow compared to the lower layer. With low flows in the upper layer, it was difficult to have a good streak photograph to represent the flow pattern. The contribution of the upper layer to the composite Froude number G was small. ***Figure 5.17*** is a graphical plot of average interface position over each minute for the experiment #7. The variation of the individual layer Froude numbers as well as the composite Froude number can be found in ***figures 5.18*** and ***5.19*** respectively. It could be seen that from figure 5.17, the interface positions at various times are almost horizontal because the exit of the channel is submerged.

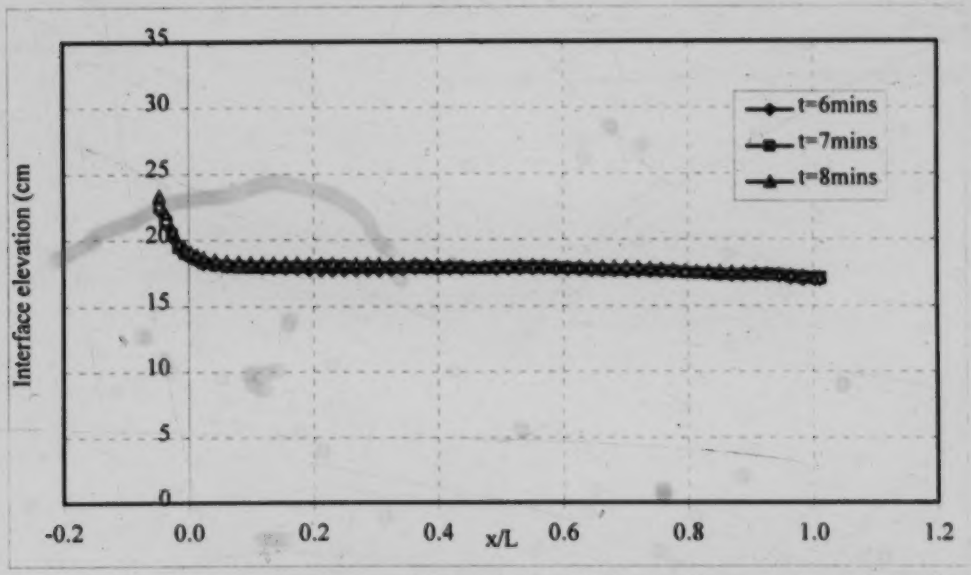

Figure 5.17 Average interface positions at t = *6,7,8 mins* for experiment #7 with the flow rate curve shown in figure 5.8. Gate opening d=*22cm* and H=*30cm*.

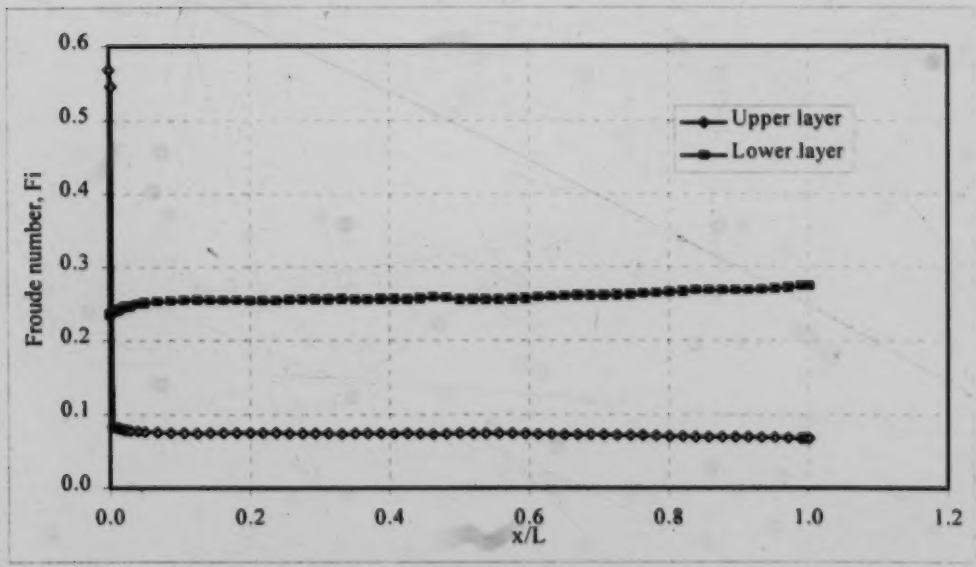

Figure 5.18 Froude numbers of the upper and lower layers in experiment #7 at t=*7 minutes*. Gate opening d=*22cm* and H=*30cm*.

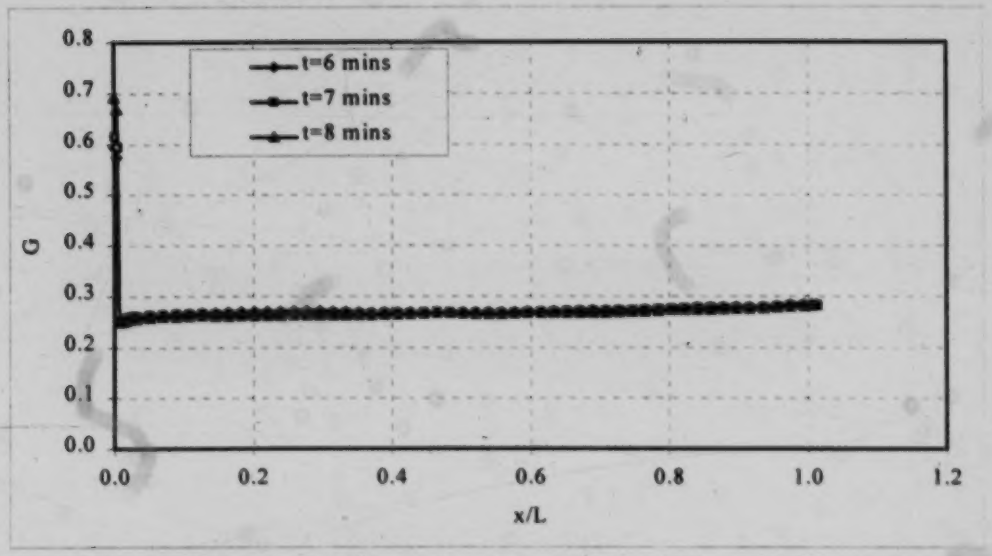

Figure 5.19 Composite Froude number for experiment #7 at *t=6,7,8 minutes*. Gate opening *d=22cm* and *H=30cm*.

From the graphical plot of Froude numbers for the upper and the lower layers in ***figure 5.18*** as well as the composite Froude number in ***figure 5.19***, it is obvious that the contribution of upper layer in G is small except very close to the gate where small thickness of the upper layer leads to a large F_1 even though the upper layer has very small flow rate. The magnitude of the Froude numbers at the gate is right but because no correction was applied for the circulating region in the upper layer, there is that unrealistic difference the graphical plot. There is also the possibility of introducing a huge error in evaluating the composite Froude number at the gate if the upper layer thickness is small for an insignificant amount of flow in that layer. The Froude number in the lower layer decreases left of the gate and the peaks close to the gate is due to the upper layer. Plots of composite Froude number for the rest of the experiments can are shown in ***figures 5.20*** and ***5.21***.

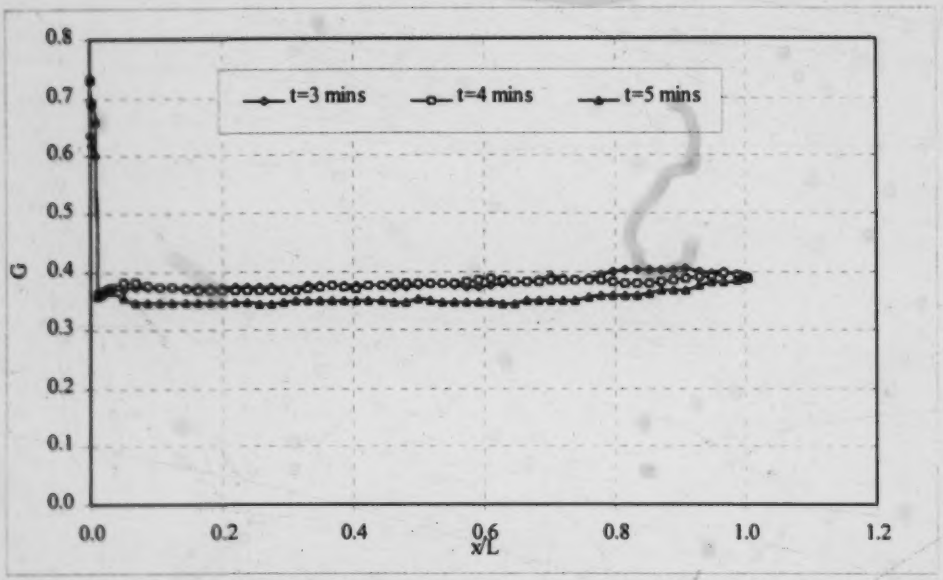

Figure 5.20 Composite Froude number for experiment #8 at *t=3,4,5 minutes*. Gate opening *d=14cm* and *H=30cm*.

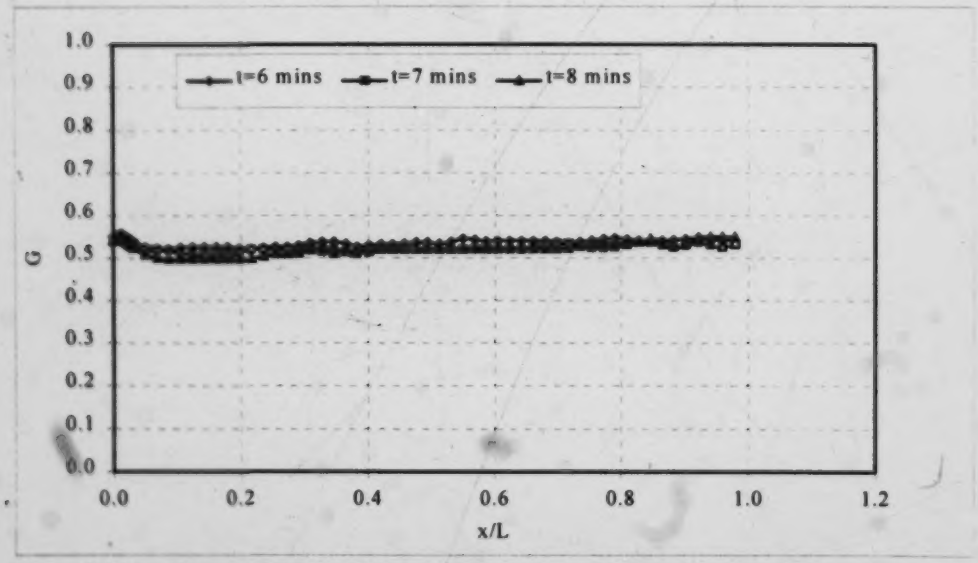

Figure 5.21 Composite Froude number for experiment #9 at *t=6,7,8 minutes*. Gate opening *d=10cm* and *H=30cm*. (Arrested flow was observed).

The upper layer thickness at the gate for situations where the upper layer was less than 0.6 *cm* were neglected. This was necessary because the gate had a thin black rubber stripe of thickness 0.3 *cm* at its leading edges which was very difficult to distinguish from that small upper layer. The idea of discarding the upper layer in such cases was supported by flow rate values, which were less than 7% of the flow in the lower layer. For experiment #9, arrested flow was observed, the upper layer thickness at the gate was 0.37 *cm*. With consideration that the leading edge of the gate has a thickness of 0.3 *cm*, the upper layer thickness can in fact be neglected. This can introduce a possible error in the calculation of the composite Froude number because it is only the contribution from the lower layer which was used in the computation. It is also a contradiction to the composite Froude number formulation because the flow rate curve indicates that there is an insignificant amount of flow in the upper layer which should be included in the composite Froude number evaluation. The flow rate curve for experiment #9 indicates that the flow rate in the upper layer is 0.89 cm^2/s. The introduction of this flow rate into the formulation of the Froude number $F_1^2 = q_1^2/\left(g' y_1^3\right)$ for a small layer thickness of 0.3 *cm* will result in a large unrealistic value.

From the Appendix, it could be seen that the flow rate curve for experiment #8 where the gate opening d=*14cm* indicates that the flow was being arrested. However experiment #9 is a complete arrested flow and the magnitude of composite Froude number required to arrest the flow is quite small (G ~0.55-0.64). In fact the composite Froude number G in these cases were contributed only by the Froude number F_2 in the lower layer.

5.3 Barotropic Forcing Experiments with Elevated Channel Bed

The pump was switched on at approximately *3* to *4* minutes after the release of the gate. The duration for the pump start-up was dependent on the rate of exchange flow. The upper layer once again did not have any correction for the effective flow surface. A streak photograph in ***figure 5.22*** taken whilst experiment #11 was in progress indicates an unclear streak path for the upper layer. This is due to the much smaller flow rate in the upper layer. In the lower layer however, the streak path was very clear to give an indication of the flow direction.

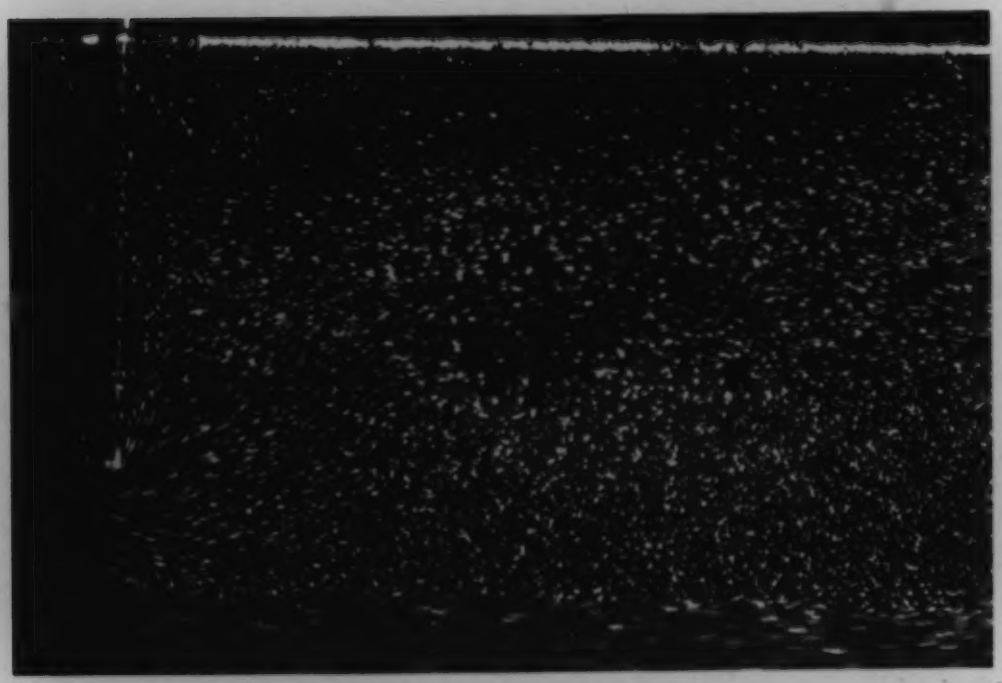

Figure 5.22 Streak photograph of experiment #11 indicating clear pattern of flow in the lower layer compared to the upper layer.

This set of experiment had an earlier pump start time because the rectangular channel bed which was raised by 7.5cm acted as a free overfall at the exit thereby accelerating the flow in the lower layer. Thus the hydraulic control shifted inside the channel which is analogous to single layer flows (see Henderson,1966) where the depth of flow at the brink $y_b \approx 0.7 y_c$. In this case y_c is the depth of flow at the critical point. ***Figure 5.23*** is a streak photograph of experiment #12 with exposure time of ¼ of a second to show the lower layer accelerating past the free overfall. Results presented later in this section indicates that there is a shift in the exit control and the new control is within a horizontal distance of $3\sim4y_c$ from the channel exit.

Experiment #13 which was part of this set of experiment rather had the elevated channel extended to the end of the right hand reservoir. The exit of the rectangular channel had composite Froude number close to unity inspite of the fact that there was a net flow between the upper and the lower layers. At the gate location however the composite Froude number had a lower value of 0.83 which indicates that the barotropic forcing have influence on the composite Froude number at the gate.

This series of experiments also had the flow rate measurements taken after *3 minutes* of the pump start-up. The steady state can be seen as a fairly horizontal section on the flow rate curve. ***Figure 5.24*** shows the flow rate curve for experiment #11 which had the gate opening *d=10.5cm* and the total depth *H=22.5cm*. Similar results for the rest of the experiments can also be found in ***Appendix*** .

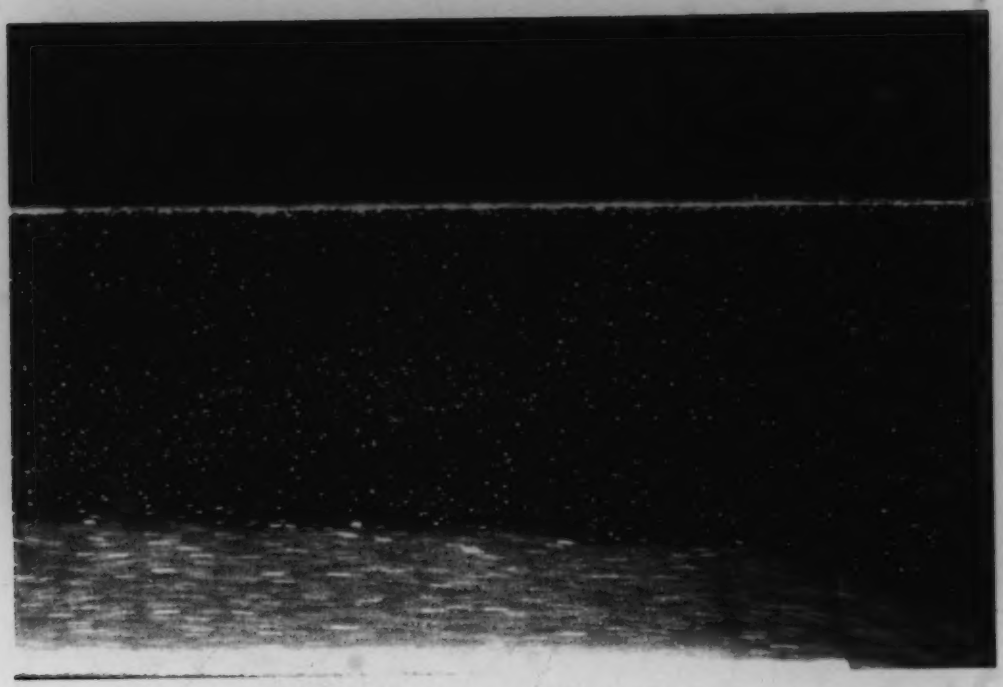

Figure 5.23 Streak photograph with exposure time of ¼ of a second for experiment#12 showing the lower layer accelerating past the free overfall whiles the upper layer is arrested.

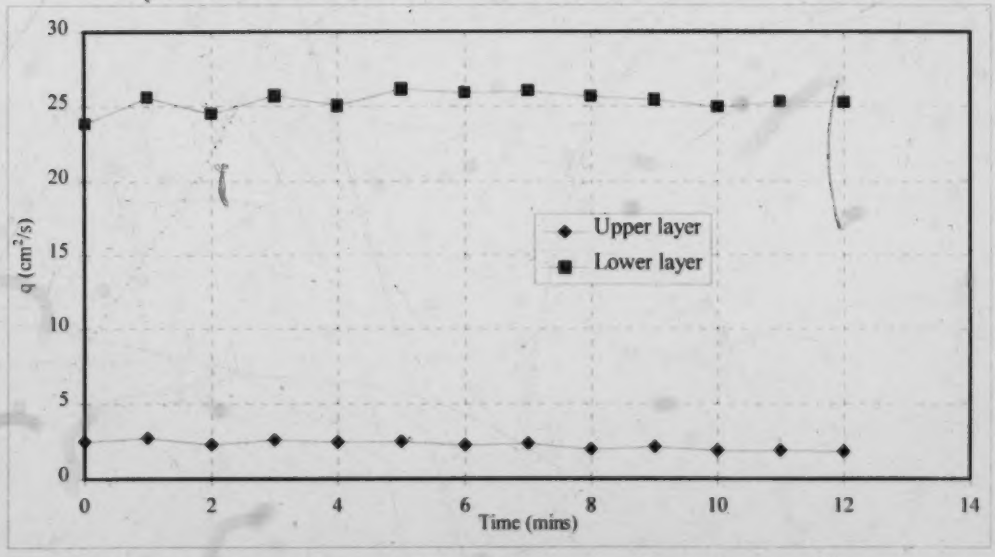

Figure 5.24: Variation of flow rate for experiment #11 after 3minutes of the pump start-up. This experiment had gate opening *d=10.5cm* and *H=22.5cm*

Experiment #12 was a case of an arrested flow. For that case, the computation of the composite Froude number was based only on the flow in the lower layer. ***Figure 5.25*** is a graphical plot of average interface position over each minute for experiment #11. The flow rate curves and interface positions for the rest of the experiments can be found in Appendix. The variation of the individual layer Froude numbers as well as the composite Froude number can be found in ***figures 5.26*** and ***5.27*** respectively.

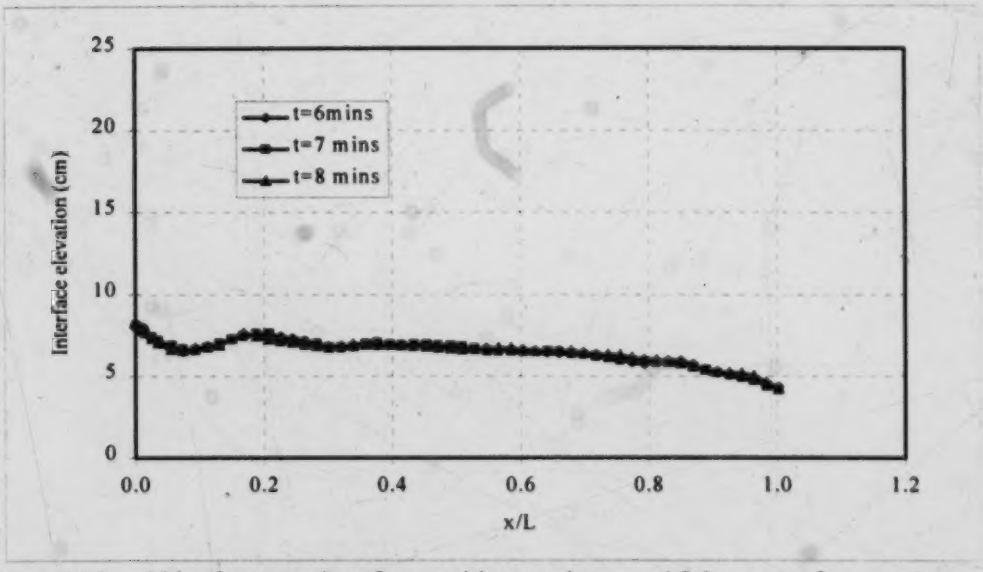

Figure 5.25: Plot of average interface positions at time *t = 6,7,8 minutes* for experiment #11 with gate opening *d=10.5cm* and *H=22.5cm*.

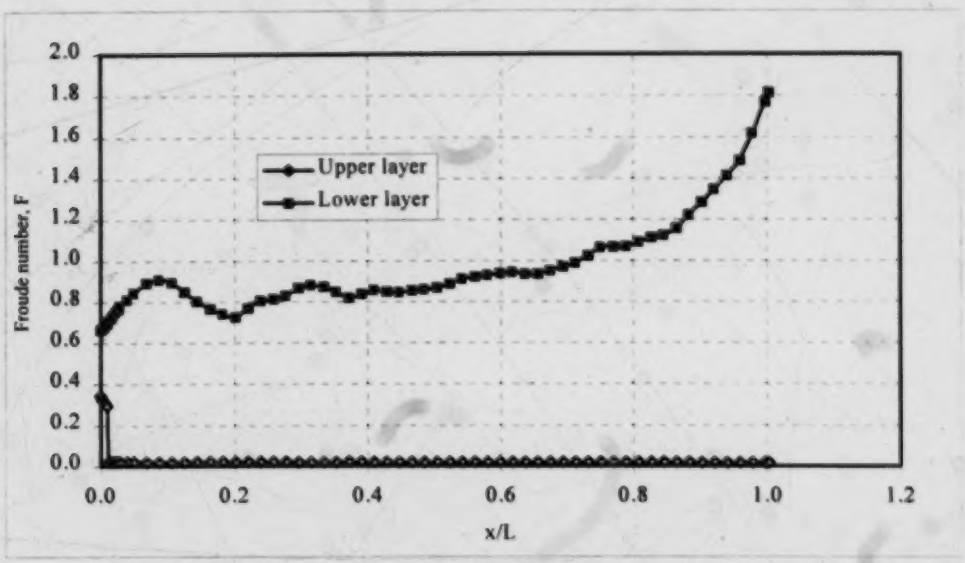

Figure 5.26 Plot of Froude numbers for the upper and lower layers for experiment #11 at time *t=7 minutes*. Gate opening *d=10.5cm* and *H=22.5cm*.

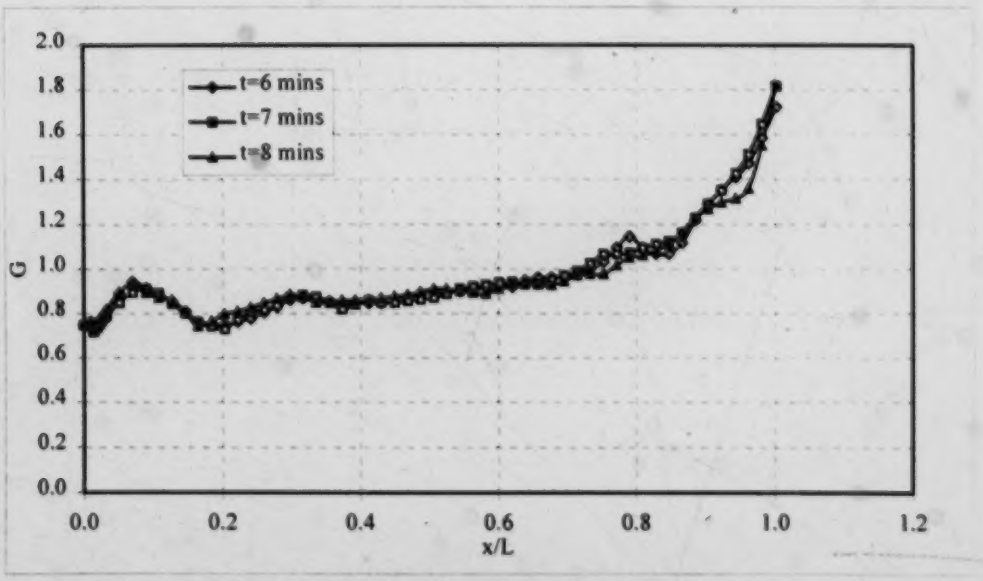

Figure 5.27: Plot of composite Froude number for experiment #11 at time *t=6,7,8 minutes*. Gate opening *d=10.5cm* and *H=22.5cm*.

The plots of composite Froude number for the rest of the experiments can be found in ***figures 5.28, 5.29*** and ***5.30*** below.

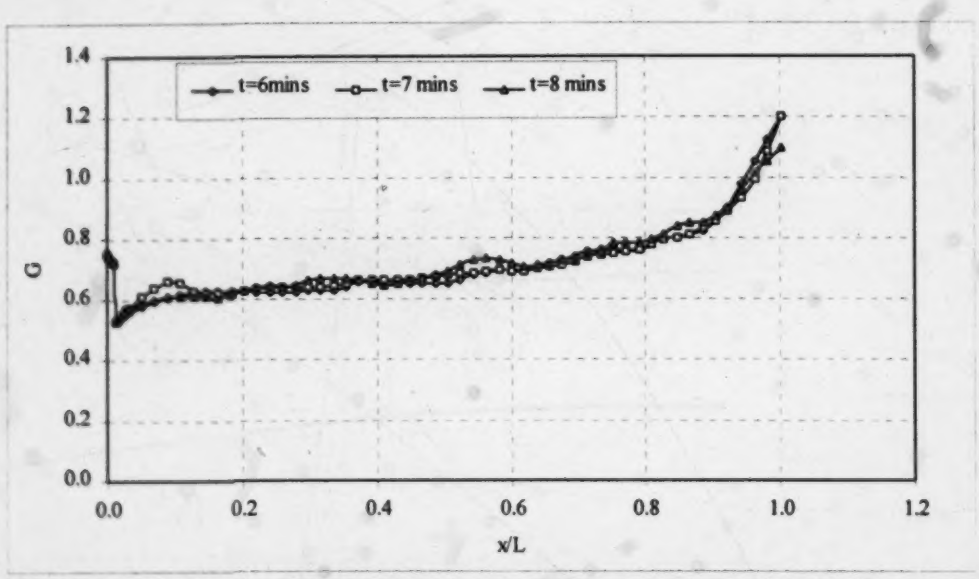

Figure 5.28 Plot of composite Froude number for experiment #10 at time *t=6,7,8* minutes. Gate opening *d=14.5cm* and *H=22.5cm*.

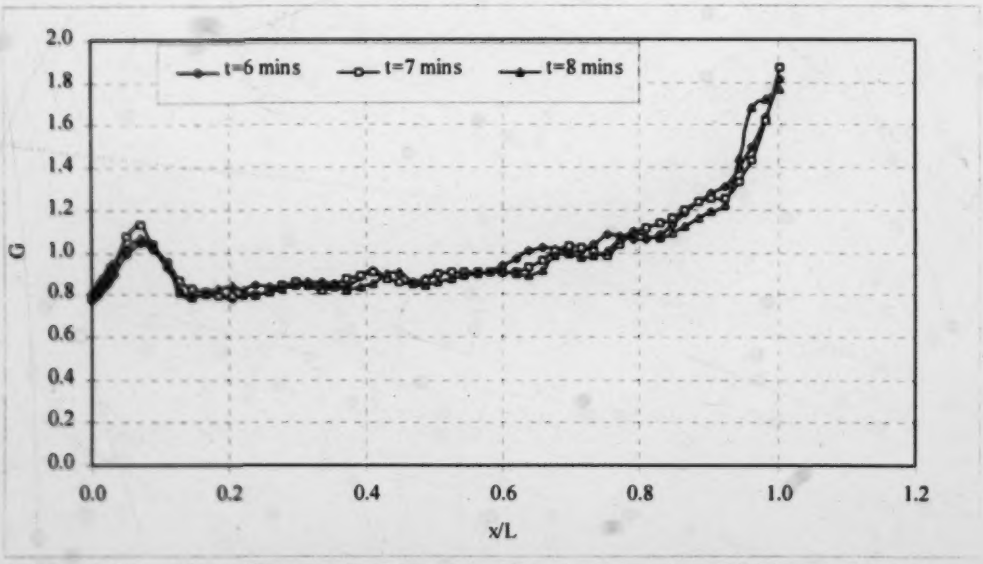

Figure 5.29 Plot of composite Froude number for experiment #12 at *t=6,7,8 minutes*. Gate opening *d=7.5cm* and *H=22.5cm*. (Arrested flow was observed.)

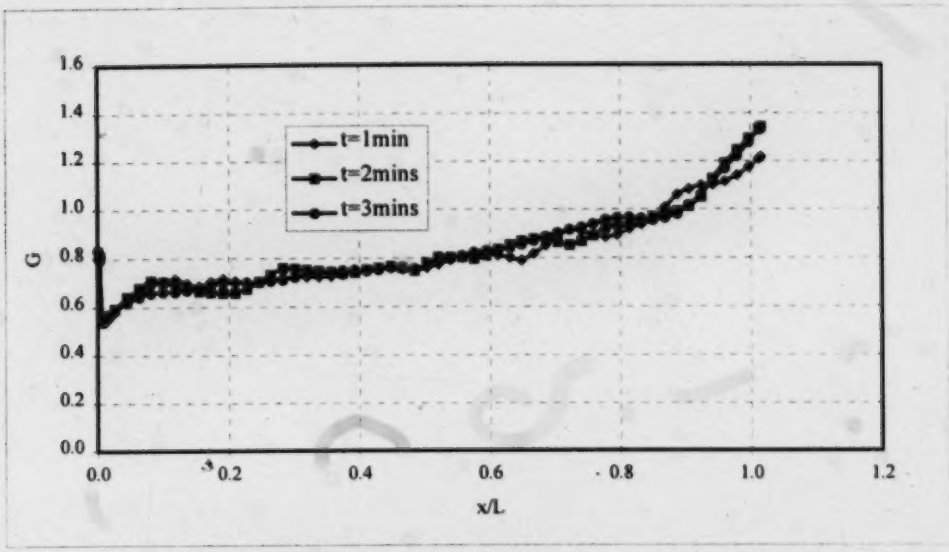

Figure 5.30 Plot of composite Froude number for experiment #13 at *t=1,2,3 minutes*. Gate opening *d=14.5cm* and *H=22.5cm*.

From plots of the composite Froude number, for experiments #10, #11 and #12, it could be seen that the hydraulic control has shifted from the channel exit because of the free overfall. Experiment #10 however, did not have a significant shift of hydraulic control from the overfall. It is due to the fact that, the upper layer flow rate was higher than those in experiments #11 and #12. This resulted in a bigger lower layer depth contributing to lower Froude numbers as compared to experiments #11 and #12. Using the averaged interface position graphs in the ***Appendix*** as well as ***figures 5.27*** and ***5.29*** for experiments #11 and #12, it could be shown that the shift of the hydraulic control from the free overfall is in the range of 17-23cm. This confirms the open channel flow relation which states that the shift can be located at a distance of $3\sim4y_c$ for a free

overfall. The value of y_c can be identified from the interface plots once the location where the composite Froude number is unity has been found.

Arrested flow was observed for experiment #12. The flow rate curve shown in ***figure 5.31*** indicates that there is an insignificant amount of flow. However the upper layer had thickness of approximately 0.5*cm*. This was neglected as already discussed in ***section 5.2.1***. A streak photograph in ***figure 5.32*** taken with an exposure time of ¼ of a second for the same experiment depicts that, the upper layer is indeed arrested. The two-layer flow for experiment #12 simply becomes one-layer with gravitational acceleration g replaced by reduced gravity g'. A plot of internal energy in ***figure 5.33*** for experiment #12 is similar to a single layer flow and the depth at the point of minimum internal energy is the same for the plotted values of the composite Froude number along the channel.

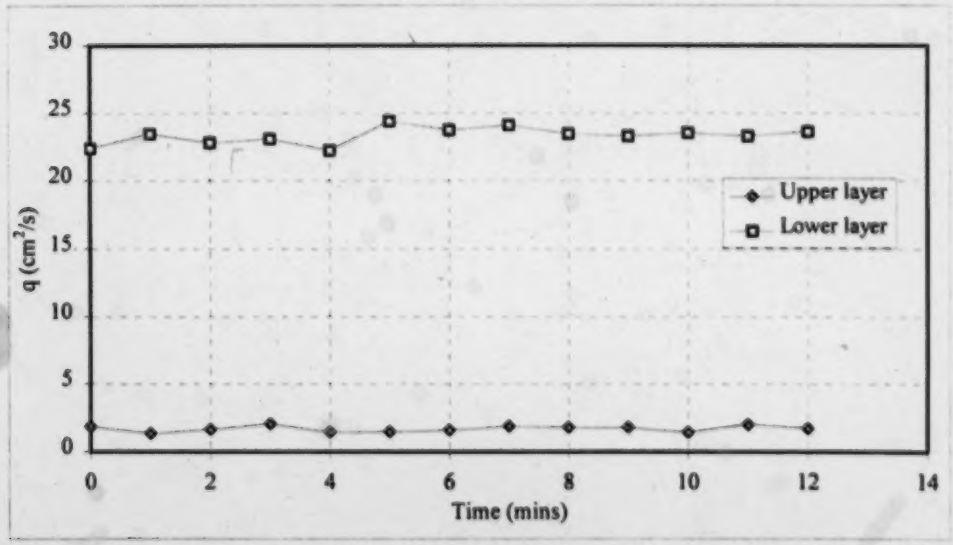

Figure 5.31 Variation of flow rate experiment #12. Gate opening d=7.5 and H=22.5*cm*. (There is an arrested flow for the upper layer).

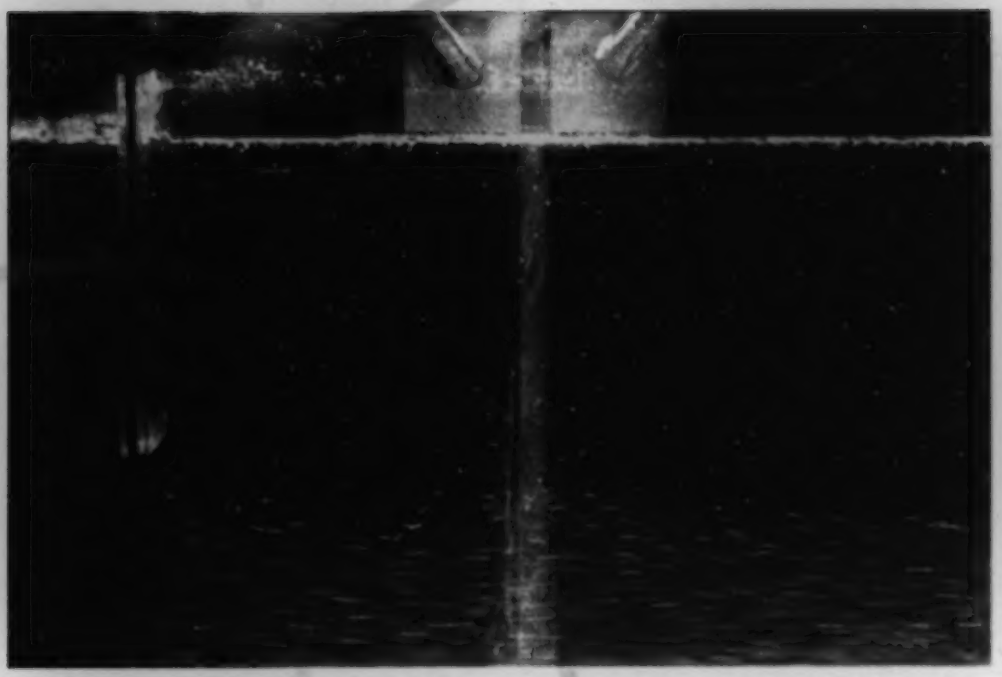

Figure 5.32 Streak photograph with exposure time of ¼ of a second for experiment #12 showing arrested flow at the gate.

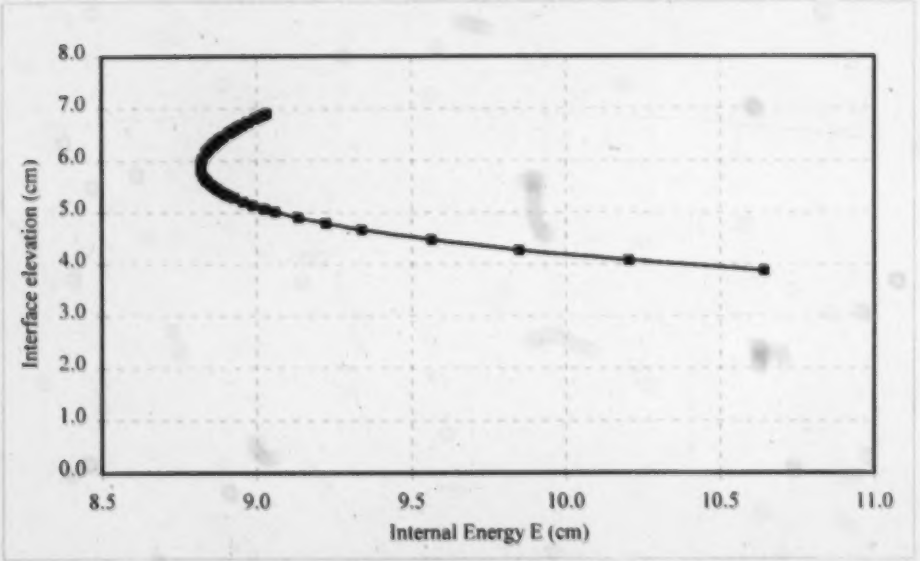

Figure 5.33 Internal Energy diagram for experiment #12. Gate opening $d=7.5cm$ and $H=22.5cm$. (Arrested flow was observed.)

5.4 Detailed Results of all the Experiments

Tables 5.1, 5.2 and ***5.3*** summarizes all the experiments together with their hydraulic control parameters. These detailed results represent the values which are characteristic of each experiment. For each experiment, the values were chosen from any of the steady state measurements.

Experiment #	Gate location					Channel exit				
	Upper layer y_1 (cm)	Lower layer y_2 (cm)	F_1	F_2	G	Upper layer y_1 (cm)	Lower layer y_2 (cm)	F_1	F_2	G
1	10.1	12.0	0.70	0.54	0.88	21.7	8.3	0.22	0.94	0.96
2	7.8	11.2	0.77	0.44	0.88	23.5	6.5	0.14	1.00	1.01
3	7.1	10.0	0.83	0.50	0.97	23.9	6.1	0.14	1.04	1.05
4	5.5	8.5	0.89	0.46	1.00	25.4	4.4	0.08	1.23	1.24
5	3.9	7.1	1.14	0.46	1.23	25.9	4.1	0.06	1.06	1.06
6	2.6	5.5	1.22	0.38	1.28	27.1	3.0	0.03	0.97	0.98

Table 5.1: Hydraulic parameters of non-barotropic forcing experiments.

Experiment #	Gate location					Channel exit				
	Upper layer y_1 (cm)	Lower layer y_2 (cm)	F_1	F_2	G	Upper layer y_1 (cm)	Lower layer y_2 (cm)	F_1	F_2	G
7	3.1	18.9	0.57	0.23	0.62	12.9	17.1	0.07	0.26	0.28
8	0.9	13.1	0.64	0.35	0.73	17.7	12.3	0.00	0.39	0.39
9	0.37^{α}	9.6	0.00	0.55	0.55	20.3	9.7	0.00	0.54	0.54

α: *values of upper layer thickness less than 0.6cm at the gate location were considered negligible (this case was considered as an arrested flow).*

Table 5.2 Hydraulic parameters of barotropic forcing experiments without exit control.

Experiment #	Gate location					Channel exit				
	Upper layer y_1 (cm)	Lower layer y_2 (cm)	F_1	F_2	G	Upper layer y_1 (cm)	Lower layer y_2 (cm)	F_1	F_2	G
10	3.8	10.7	0.57	0.49	0.75	17.1	5.4	0.06	1.38	1.38
11	2.3	8.2	0.35	0.66	0.75	18.3	4.2	0.01	1.81	1.81
12	0.5[α]	7.0	0.00	0.77	0.77	18.6	4.0	0.00	1.82	1.82
13[ψ]	4.0	10.6	0.66	0.51	0.83	16.9	5.6	0.07	1.30	1.30

α: *values of upper layer thickness less than 0.6cm at the gate location were considered negligible (this case was considered as an arrested flow).*

ψ: *this experiment had the elevated channel bed extended to the end of the tank*

Table 5.3 Hydraulic parameters of barotropic forcing experiments with elevated channel bed.

From the detailed results in ***table 5.1*** which represents flow without barotropic forcing, it could be seen that the composite Froude number G, at the gate is in the range of 0.9-1.3. The values are in fact close to 1 which suggests that the gate is a hydraulic control for non-barotropic forcing. The channel exit also have the values of composite Froude number in close to 1.

Barotropic experiments without exit control in ***table 5.2*** also had composite Froude number in the range of 0.5-0.7. The exit of the channel for this particular set of experiments which had a submerged exit had composite Froude numbers in the range 0.3-0.5.

Table 5.3 gives the values of composite Froude number at in the range of 0.7-0.8 at the gate for experiments #10, #11 and #12. The exit of the rectangular channel also had composite Froude numbers in supercritical range of 1.1-1.8. Finally experiment #13

which had the elevated channel bed extended to the right hand reservoir had value of composite Froude number of 0.83 at the gate and 1.3 at the channel exit.

Chapter 6

APPLICATIONS OF TWO-LAYER FLOW THROUGH AN OPENING IN ENGINEERING

6.1 Exchange Flow through Doorways and Windows

When the surroundings of a building is cooler (or warmer) than the rooms in the building, the opening of a window or doorway will result in an exchange of cold and warm air. This can also be the case for cold storage rooms such as meat and ice storage facilities for which the surroundings are warmer. In all these cases, the doorway or window acts as a control in which a continuous exchange of thermally stratified flow takes place. Knowledge of the control points help in determining the mechanisms of control and hence the flow rate from each layer. Areas of application is in the design of rooms and quarantine wards in hospitals where a high level of importance is attached to the air movement control to prevent the exchange of contaminated air to areas where infection may be caused.

There are also situations where in order to prevent the transfer of air across doorways due to a difference in temperature, it is necessary (as in operating rooms) to supply excess air to the room which requires to be isolated. This imposed flow (called barotropic forcing) through the doorway will counteract the flow of the incoming contaminated air. This is a typical arrested flow situation in which a knowledge of the effects of barotropic forcing is very helpful in determining the mechanisms of control and the amount of air required to prevent airflow across an opening.

6.2 Navigation Lock Operations

Navigation locks joining estuaries may have lock chambers with water of different densities due to the intrusion of salt water or in some cases the presence of suspended sediments and dissolved salts carried by the river into the sea. The separated chambers therefore have water of different densities and in the cause of its operation, the opening of the locks will result in an exchange flow. Exchange flows in this case lasts for a short while because the locks are lifted completely for the safe passage of ships and boats. Skimmer walls can also be used on lock filling intakes where the navigation locks separate regions of fresh and salt water. The use a skimmer wall in this manner removes the salt water, which intrudes into the fresh water basin during lock operations. The knowledge of the control of exchange flow mechanisms is therefore very important in the design of the locks.

6.3 Selective Withdrawal of Cold Water using Skimmer Walls

The economic justification for increasing the efficiency of steam-electric power generation with cool water during hot weather seasons as well as the use of cool water for drinking sometimes demands the use of skimmer walls. A skimmer wall is a submerged sluice gate structure for the purpose of withdrawing water selectively from two-layered systems. The water in the intake structure downstream from the skimmer wall is homogeneous and ideally has a temperature equal to that of the lower layer of cold water in the river or reservoir. The colder water in this case, flows through the opening at the

bottom of the skimmer wall by virtue of a head differential across the wall caused by the intake pumps.

In many cases, the skimmer is only partially effective because it withdraws water from both the lower and the upper layer. The effective means by which skimmers wall can work is at the point of supercritical withdrawal where a maximum discharge can be realized only for the lower layer. This represents the point of incipient motion where the upper layer is about to be withdrawn. The knowledge of two-layer flows under a sudden obstruction can also help in determining the maximum colder water discharge that can be withdrawn from a given intake geometry without inducing appreciable withdrawal from the upper layer of warm water.

Chapter 7

CONCLUSIONS

The experimental studies conducted with a planar sluice gate to observe the mechanisms of control has cleared the confusion over barotropic and non-barotropic forcing. There is a clear distinction for values of the composite Froude number for both situations at steady state. Flow without barotropic forcing gives the composite Froude number, G, in the range of 0.9-1. 3 at the gate location. In fact the value of the composite Froude number is close to unity which is consistent with values given in literature. The value of G was in an increasing order as the gate opening reduces. At the channel exit, the values were also noted to be in the range of 0.9-1.1. This confirms the fact that there are two controls; one at the gate and the other at the channel exit. In between the two controls, the flow remains subcritical.

For the case of barotropic forcing, two sets of experiments were performed. In all the experiments, the flow in the upper layers were in the range of *1-23%* of their respective lower layers. This range of net flow can be described as moderate to strong barotropic forcing. The first set had a subcritical flow at the channel exit whiles the other had the whole rectangular channel raised to the extent that the channel bed at the exit acted as a free overfall. In the first set of experiments for the barotropic forcing, the composite Froude number at the gate location was in the range of 0.5-0.7 while the exit which was already submerged also had values in the range of 0.3-0.5. The last set of experiments were conducted with the view of avoiding subcritical state at the channel exit which was initially thought to be having influence on the values composite Froude number at the

gate. The composite Froude numbers obtained for the last set of experiments however did not change significantly as they were in the range of 0.7-0.8. The exit at the channel in this case rather had the composite Froude numbers in the range of 1.1-1.8, which clearly shows that the exit was in a supercritical state. The experiments conducted with net flow therefore draws attention to the fact that the flow at the gate location is not critical at steady state and for that reason, depth-discharge relationship cannot be readily obtained.

Although the flow pattern curve was found to represent very well the relationship between the gate submergence and the streak path along the entire channel, there is the need to have a more comprehensive relation, which will be able to include all the variables involve in the exchange flow. Further studies on barotropic forcing through openings should also consider the flow pattern in the upper layer as a result of the net flow created by pumping the lower layer from the right hand to the left hand reservoir.

REFERENCES

Adams, E. E. and Cosler, D. J. 1988 Density exchange flow through a slotted curtain. *J. Hydr. Res.* **26**, 261-273.

Armi, L. 1986 The hydraulics of two flowing layers with different densities. *J. Fluid Mech.*, **163**, 27-58.

Armi, L. and Farmer, D. M. 1986 Maximal two-layer exchange through a contraction with barotropic net flow. *J. Fluid Mech.*, **164**, 27-51.

Baines, P. G. 1984 A unified description of two-layer flow over a topography. *J. Fluid Mech.*, **146**, 127-167.

Barr, D. I. H. and Hassan, A. M. M. 1963 Densimetric exchange flow in rectangular channels (Part II- Some observations of the structure of lock exchange flow). *La Houille Blanche*, **7**, 757-766.

Barr, D. I. H. 1963 Densimetric exchange flow in rectangular channels (Part I- Definitions, Review and Relevance to model design). *La Houille Blanche*, **7**, 739-754.

Barr, D. I. H. 1967 Densimetric exchange flow in rectangular channels (Part III- Large scale experiments). *La Houille Blanche*, **6**, 619-631.

Bormans, M. and Garrett, C. 1989 The effects of Non-rectangular cross section, friction and barotropic fluctuations on the exchange through the Strait of Gibraltar. *J. Physical Oceanography*, **19**, 1543-1557

Dalziel, S. B. and Lane-Serff, G. F. 1991 The hydraulics of doorway exchange flows. *Building and Environment*, **26**, 121-135.

Dalziel, S. B. 1991 Two-layer hydraulics: a functional approach. *J. Fluid Mech.*, **233**, 135-163.

Denton, R. A. 1987 Locating and identifying hydraulic controls for layered flow through an obstruction. *J. Hydr. Res.*, **25**, 281-299.

Farmer, D. M. and Armi, L. 1986 Maximal two-layer exchange over a sill and through the combination of a sill and contraction with barotropic flow. *J. Fluid Mech.*, **164**, 53-76.

Gibson, A. H. 1918 Experiments on the coefficient of discharge under rectangular sluice-gates. *Proc., Inst. of Civ. Engrs.*, London, England, Vol. ccvii, 427-434.

Hamblin, P. F. and Lawrence, G. A. 1990 Exhange flows between Hamilton Harbor and Lake Ontario. *Proc. of 1990 Annual Conf. of Canadian Society for Civil Eng.* V ; 140 - 148.

Harleman, D. R. F., Gooch, R. S. and Ippen, A. T. 1958 Submerged sluice control of stratified flow. *J. Hydr. Div., ASCE.* **84**(2), pp1584

Harleman, D. R. F. and Elder, R. A. 1965 Withdrawal from two-layer stratified flows. *J. Hydr. Div., ASCE.* **91**(4), 43-58.

Henderson, F. M. Open Channel Flow. 1966 *Macmillan Press.*

Jirka, G. H. 1979 Supercritical withdrawal from two-layered fluid systems (Part I: Two dimensional skimmer wall), *J. Hydr. Res.*, **17**, 43-51.

Lawrence, G. A. 1990 On the hydraulics of Boussinesq and non-Boussinesq two-layer flows. *J. Fluid Mech.*, **215**, 457-480.

Lawrence, G. A. 1993 The hydraulics of steady two-layer flow over a fixed obstacle. *J. Fluid Mech.*, **254**, 605-633.

Lide, D. R. 1998 CRC Handbook of Chemistry and Physics. 79th. Edition.

Lohmeyer, A. and Plate, E. J. 1977 Selective withdrawal from two-layer stratified flow. *Proc. of 17th. Congress, IAHR*, Baden. Vol. 1, pp: A44

Montes, J. S. 1997 Irrotational flow and real fluid effects under planer sluice gates. *J. Hydr. Engrg.*, **123**, 219-232.

Pawlak, G. & Armi, L. 1997 Hydraulics of two-layer arrested wedge flows. *J. Hydr. Res.* **35**(5), 603-618.

Pratt, L. J. 1986 Hydraulic control of sill flow with bottom friction. *J. Phys. Oceanogr.*, **16**, 1970 – 1980

Rajaratnam, N., and Humphries, J. A. 1982 Free flow upstream of vertical sluice gates. *J. Hydr. Res.*, **20**(5), 427-437.

Rajaratnam, N. 1977 Free flow immediately below sluice gates. *J. Hydr. Div. ASCE*, **103**(4), 345-351.

Rajaratnam, N. and Johnston, G. Intrusion at outlets in stratified flows (Techn. report)

Schijf, J. B. and Schonfeld, J. B. 1953 Theoritical considerations on the motion of salt and fresh water. *Minnesota Intl. Hydraulics Conv., IAHR, ASCE*, pp. 321-333.

Shaw, B. H. and Whyte, W. 1974 Air movement through doorways - the influence of temperature and its control by forced airflow. *J. Inst. Heat Vent. Eng.* **42**, 210-218.

Steven, C. and Coates, M. 1994 Applications of maximized cross-correlation technique for resolving velocity fields in laboratory experiments. *J. Hydraul. Res.*, **32**, 195-212.

Yih, C. 1969 A class of solutions for steady stratified flows. *J. Fluid Mech.*, **36**, 75-85.

Zhu, D. Z. 1996 Exchange flow through a channel with an underwater sill. Ph.D. Thesis, Department of Civil Engineering, University of British Columbia.

Zhu, Z. and Lawrence, G. A. 1996 Exchange flow through a channel with an underwater sill Dynamics of atmospheres and oceans. **24**, 153-161.

Zhu, D. Z. and Lawrence, G. A. 1998 Non-hydrostatic effects in layered shallow water flows. *J. Fluid Mech.*, **355**, 1-16.

Zhu, D.Z. and Lawrence, G. A. 1999 Hydraulics of exchange flows. *Submitted to Journal of Hydraulic Engineering (ASCE).*

APPENDIX

Variation of Flow Rate and Average Interface Position

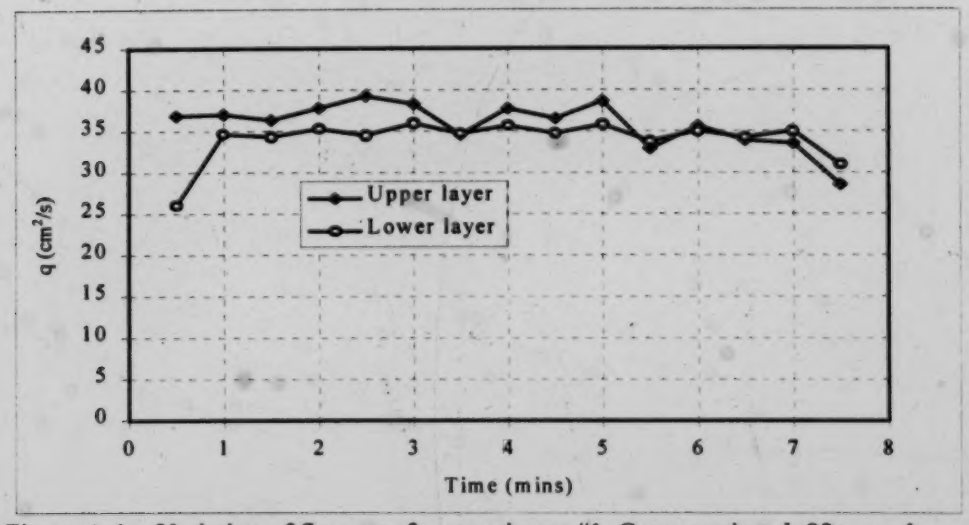

Figure A-1: Variation of flow rate for experiment #1. Gate opening d=22cm and H=30cm.

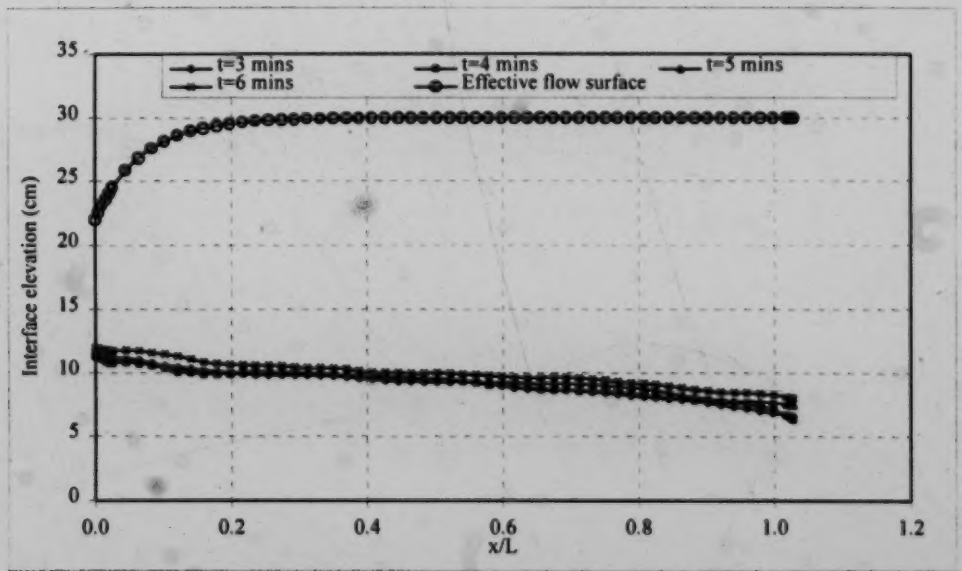

Figure A-2: Average interface position for experiment #1. Gate opening d=22cm and H=30cm.

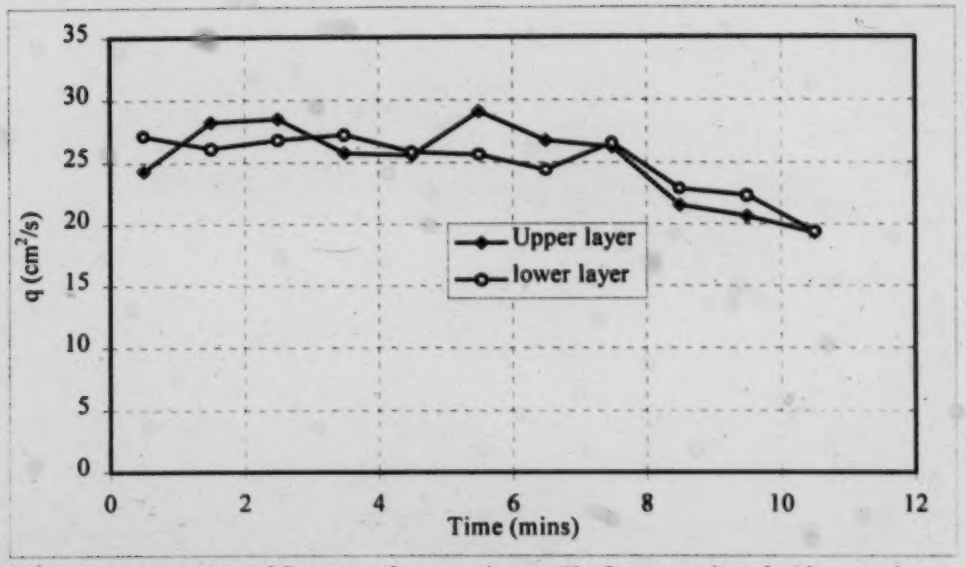

Figure A-3: Variation of flow rate for experiment #2. Gate opening *d=19 cm* and *H=30 cm.*

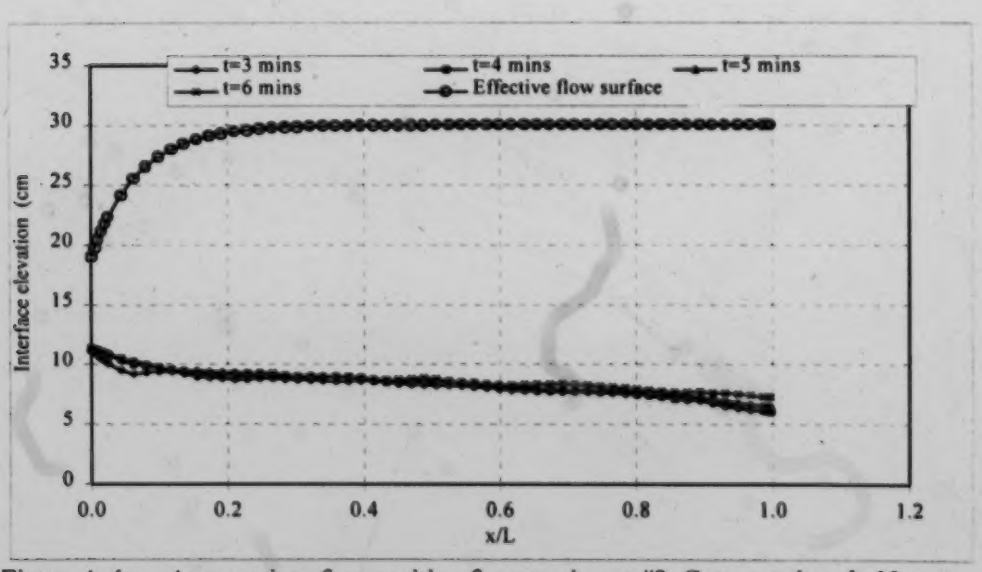

Figure A-4: Average interface position for experiment #2. Gate opening *d=19 cm* and *H =30 cm.*

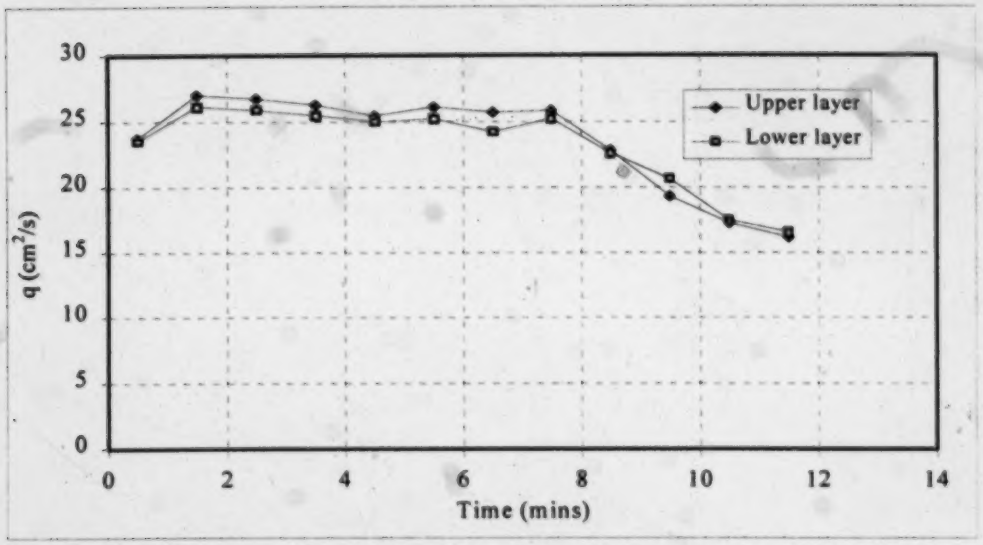

Figure A-5: Variation of flow rate for experiment #3. Gate opening *d=17 cm* and *H=30 cm*.

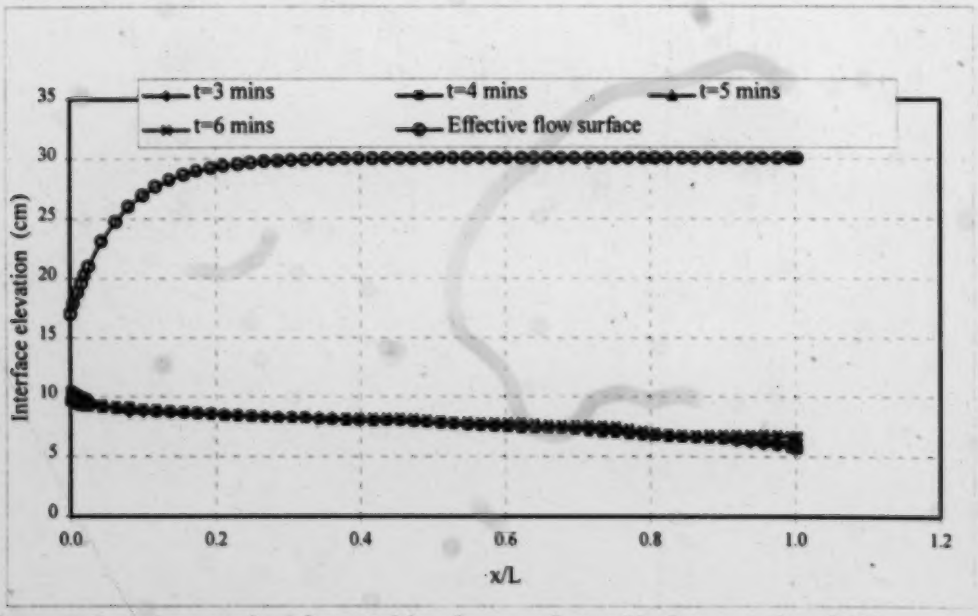

Figure A-6: Average interface position for experiment #3. Gate opening *d=17 cm* and *H=30 cm*.

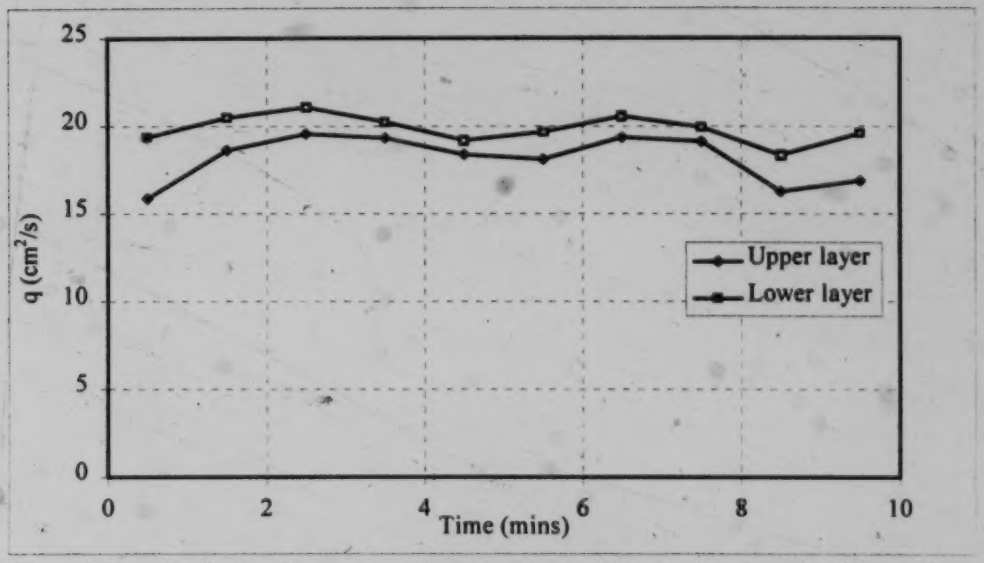

Figure A-7: Variation for flow rate for experiment #4. Gate opening *d=14 cm* and *H =30 cm.*

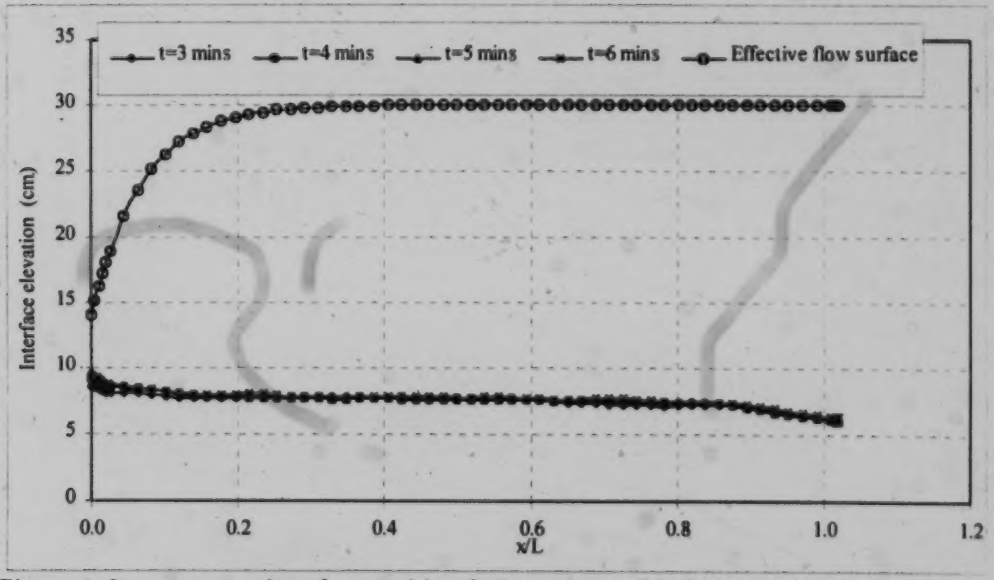

Figure A-8: Average interface position for experiment #4. Gate opening *d=14 cm* and *H =30 cm.*

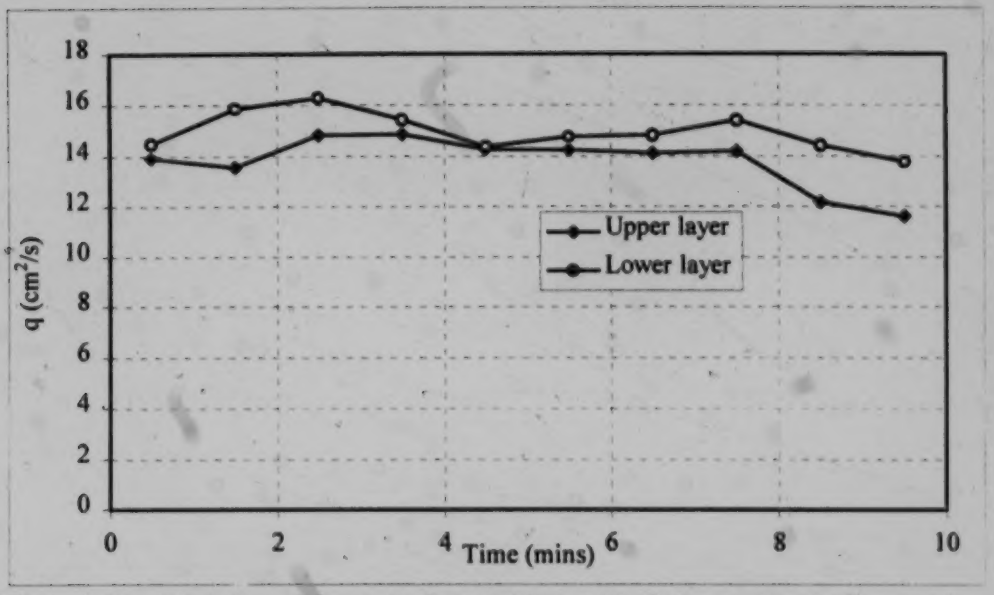

Figure A-9: Variation of flow rate for experiment #5. Gate opening *d=11 cm* and *H=30 cm*

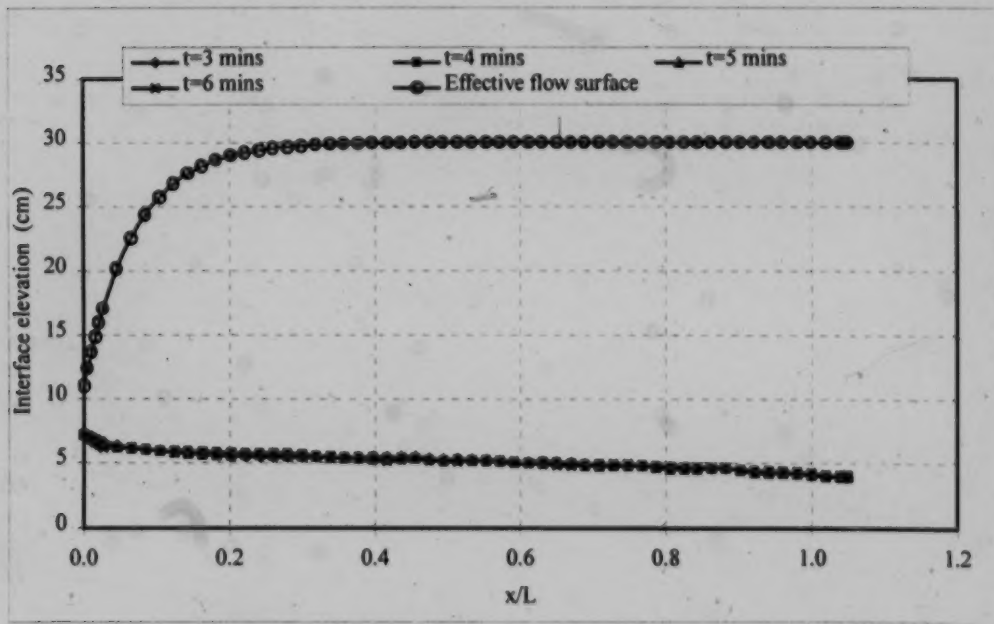

Figure A-10: Average interface position for experiment #5. Gate opening *d=11 cm* and *H=30 cm*.

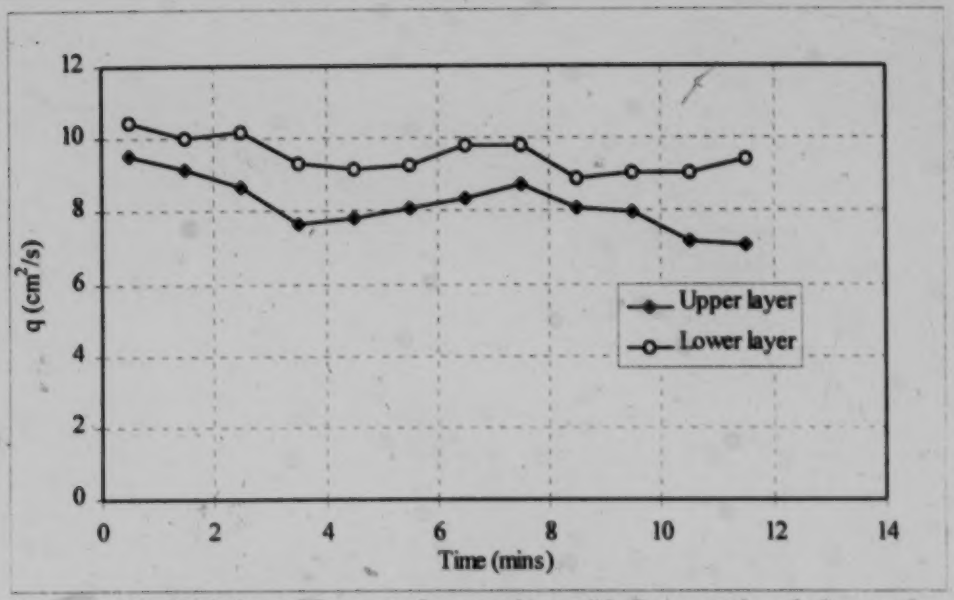

Figure A-11: Variation of flow rate for experiment #6. Gate opening *d=8 cm* and *H=30 cm.*

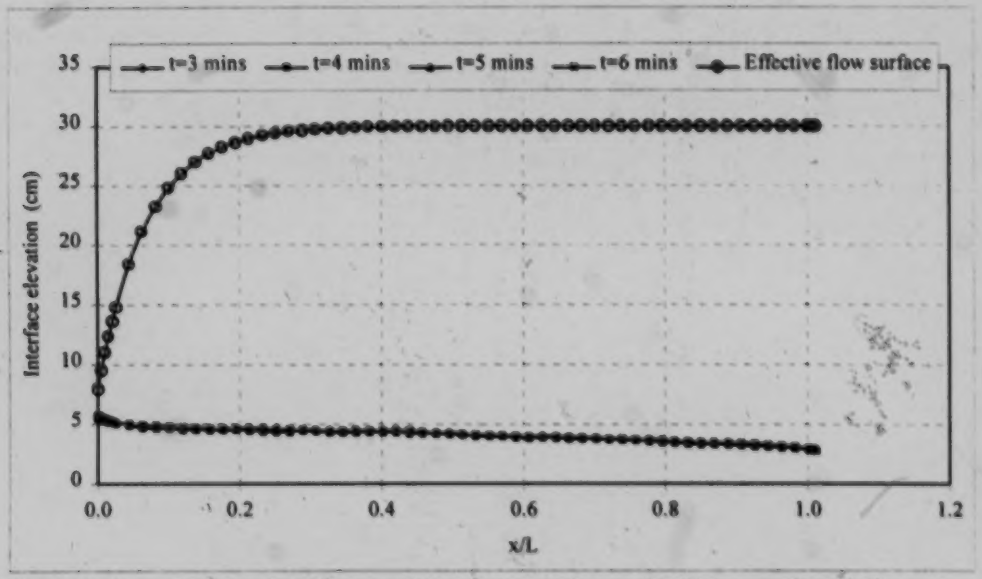

Figure A-12: Average interface position for experiment #6. Gate opening *d=8 cm* and *H=30 cm.*

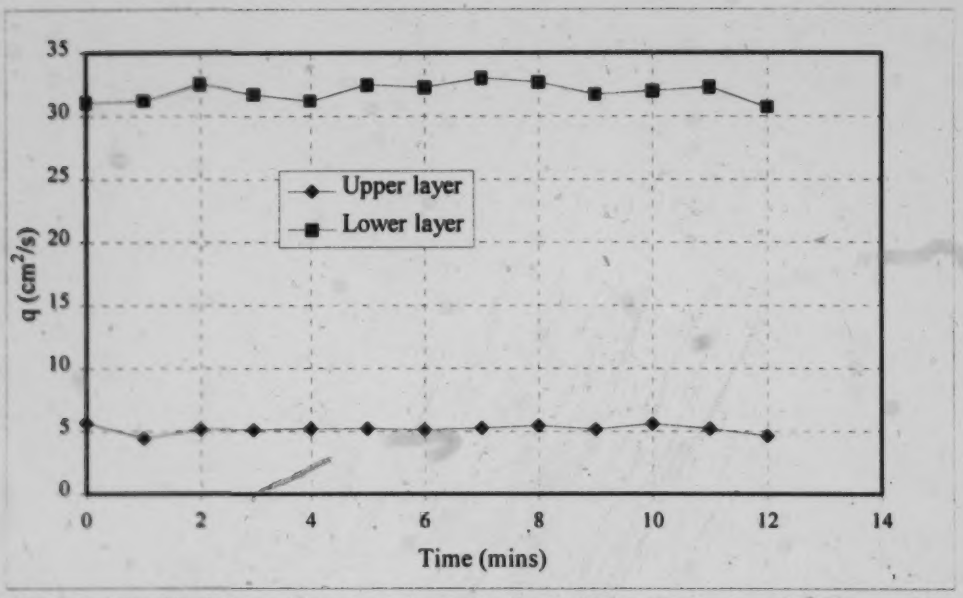

Figure A-13: Variation of flow rate for experiment #7. Gate opening *d=22 cm* and *H=30cm*.

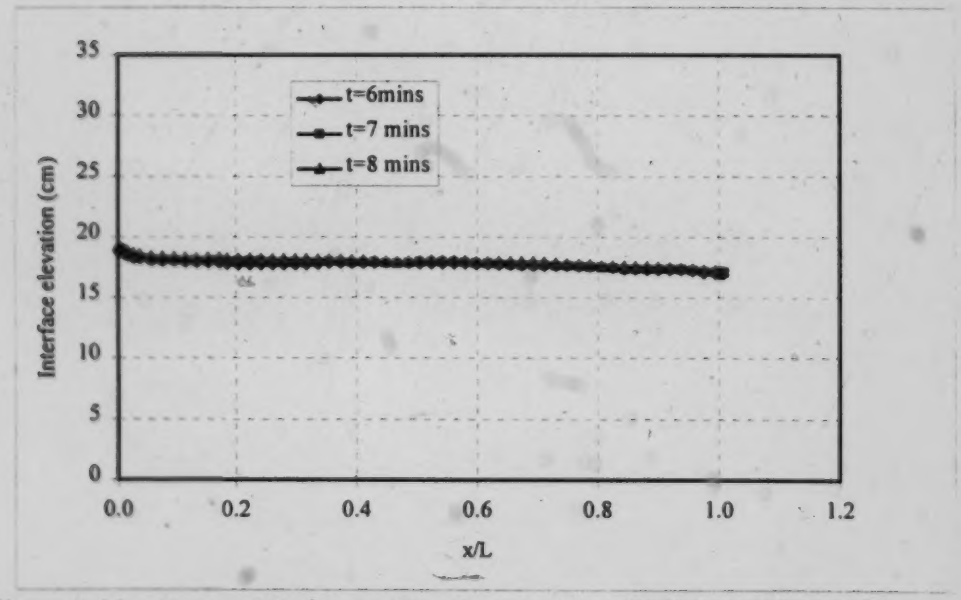

Figure A-14: Average interface position for experiment #7. Gate opening *d=22 cm* and *H=30 cm*.

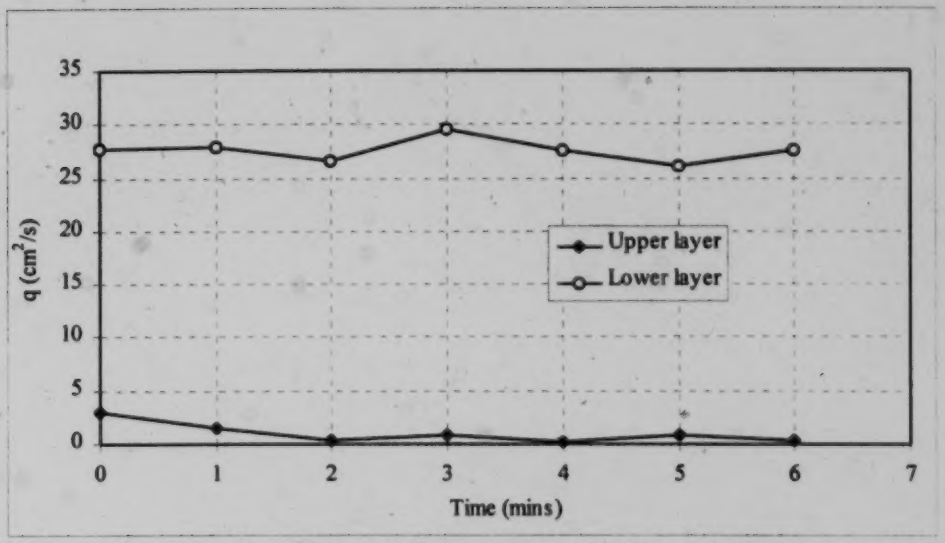

Figure A-15: Variation of flow rate for experiment #8. Gate opening *d=14 cm and H=30 cm.*

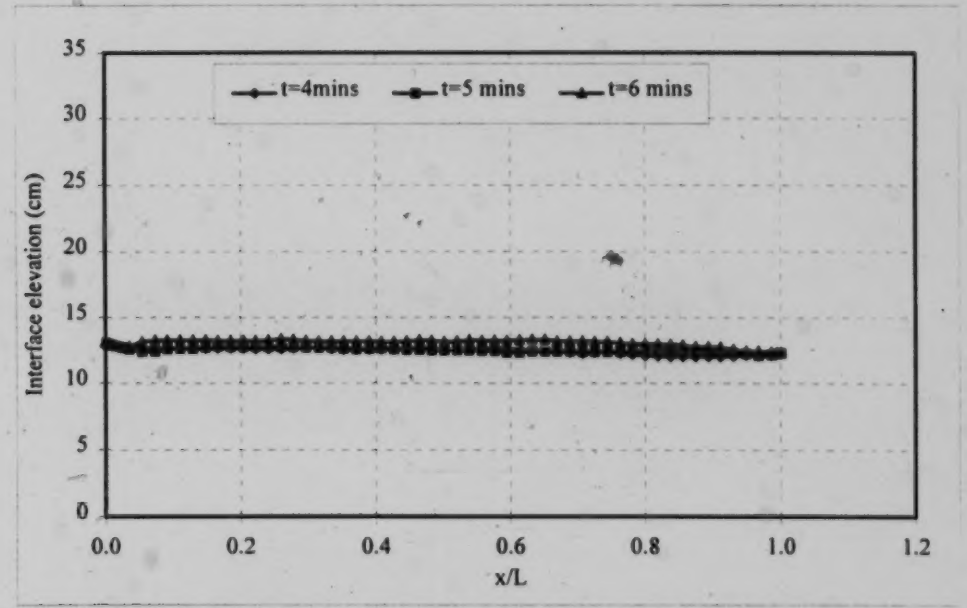

Figure A-16: Average interface position for experiment #8. Gate opening *d=14 cm and H=30 cm.*

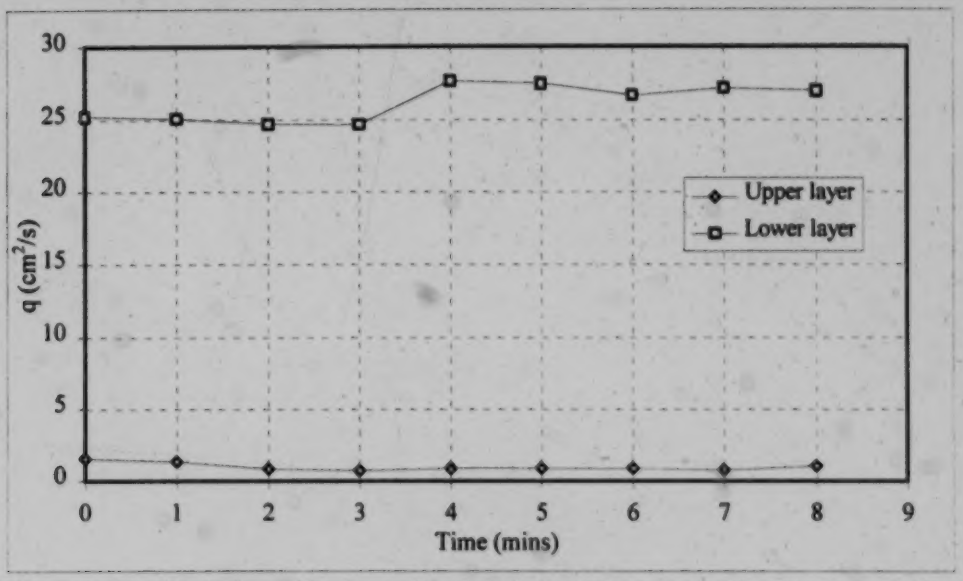

Figure A-17: Variation of flow rate for experiment #9. Gate opening *d=10 cm* and *H=30 cm*.

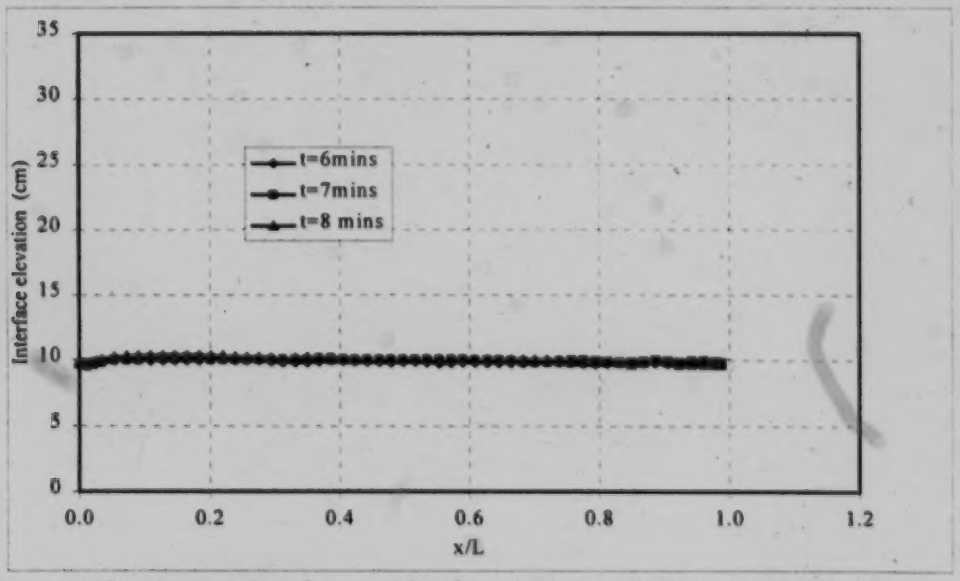

Figure A-18: Average interface position for experiment #9. Gate opening *d=10 cm* and *H=30 cm*.

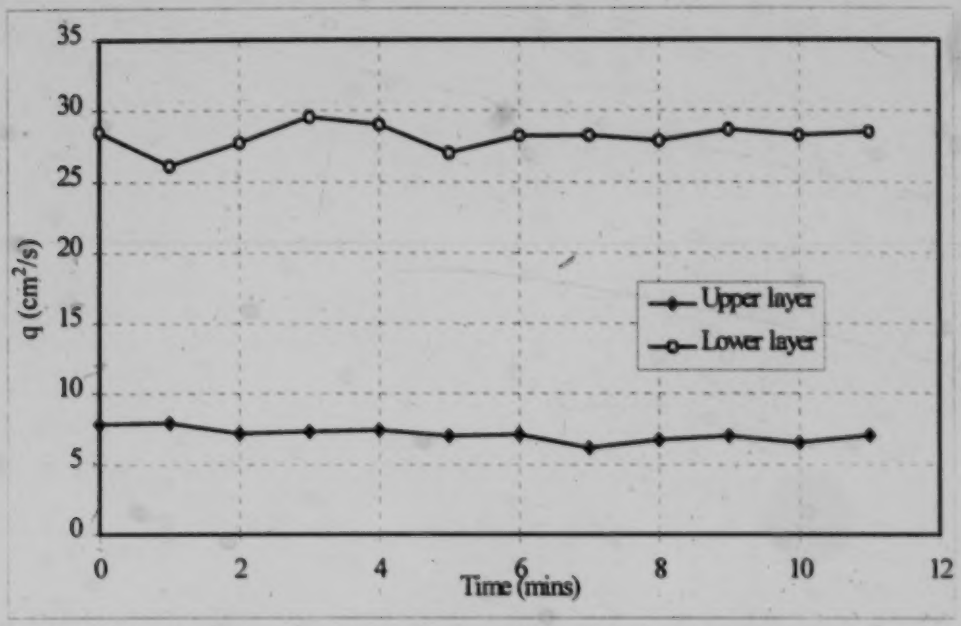

Figure A-19: Variation of flow rate for experiment #10. Gate opening *d=14.5 cm* and *H=22.5 cm.*

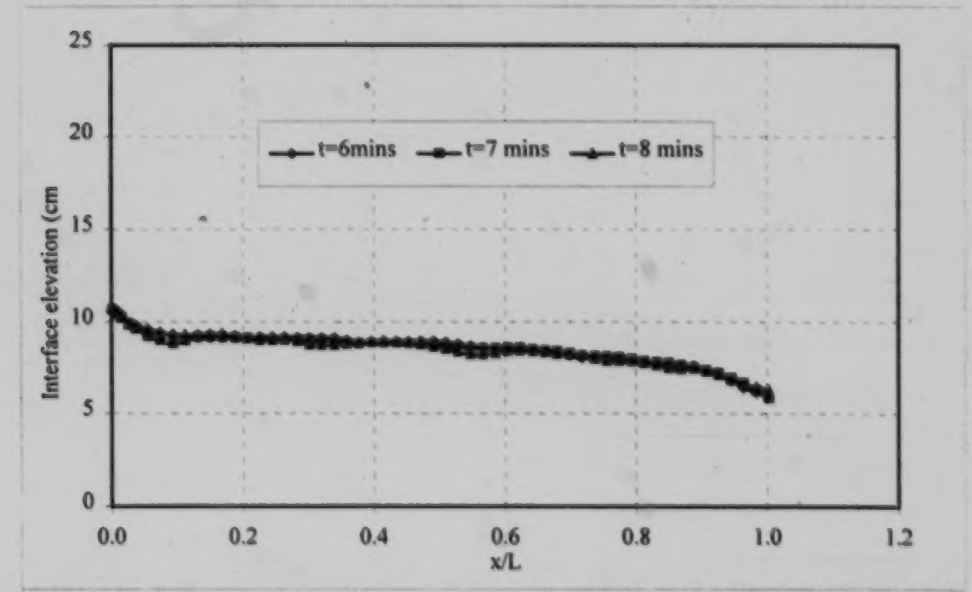

Figure A-20: Averaged interface position for experiment #10. Gate opening *d=14.5 cm* and *H=22.5 cm.*

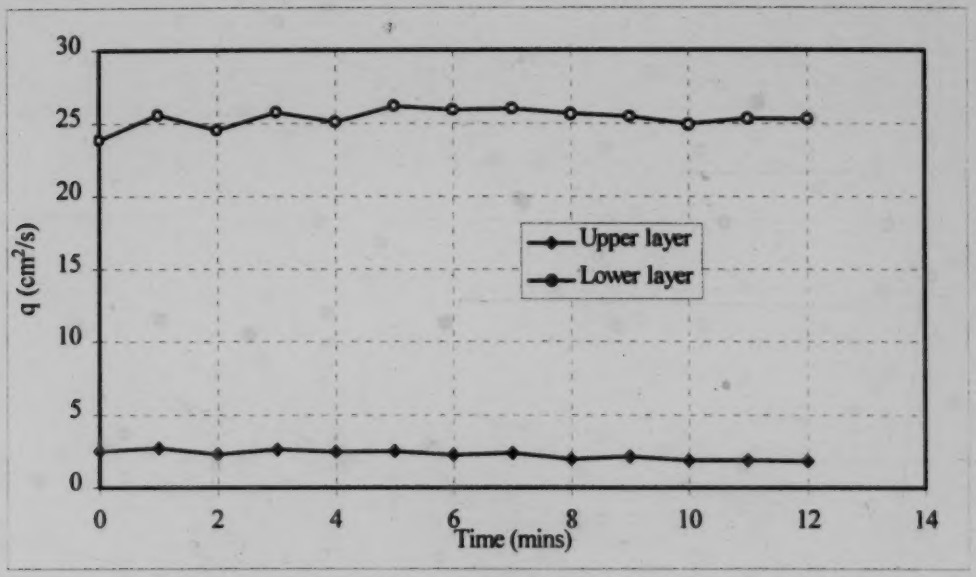

Figure A-21: Variation of flow rate for experiment #11. Gate opening *d=10.5 cm and H=22.5 cm.*

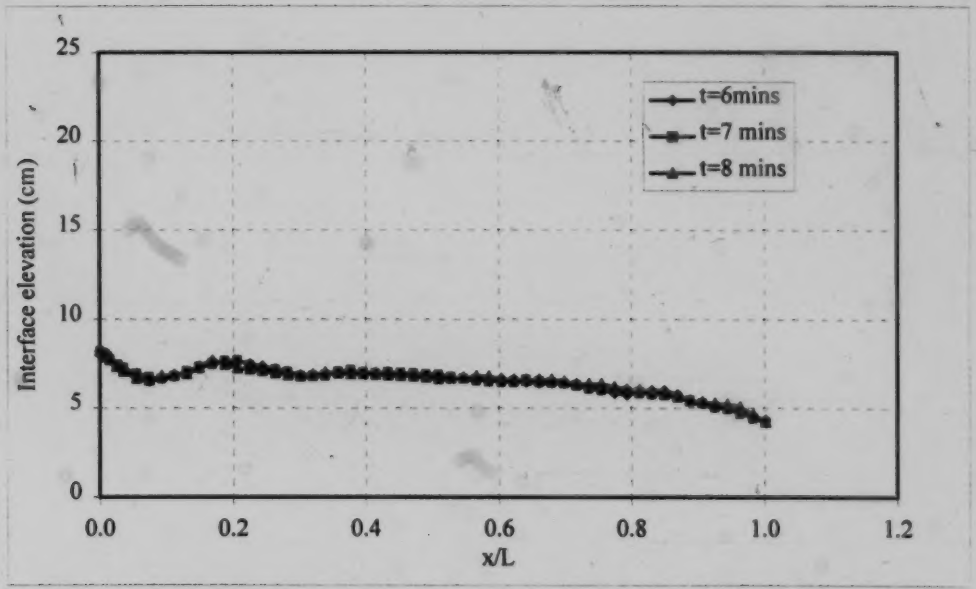

Figure A-22: Average interface position for experiment #11. Gate opening *d=10.5 cm* and *H=22.5 cm.*

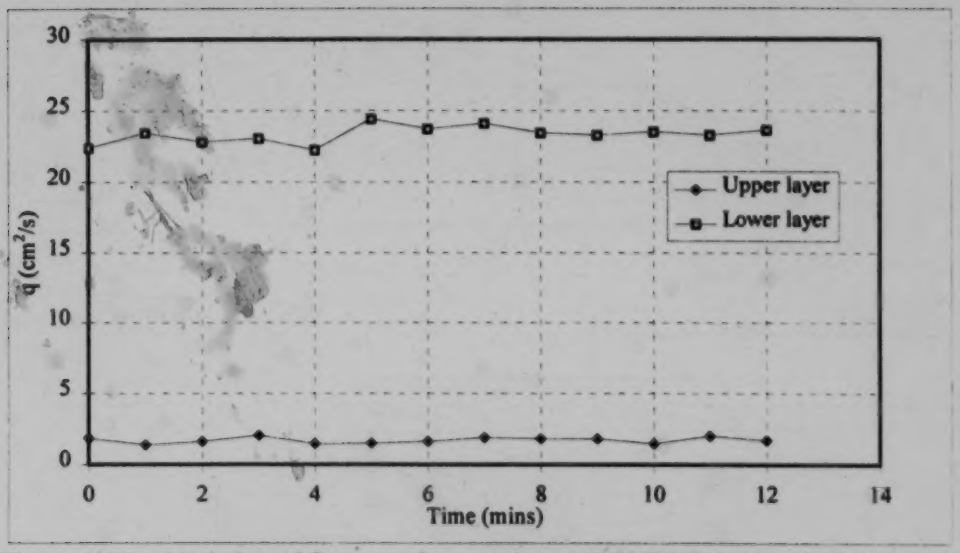

Figure A-23: Variation of flow rate for experiment #12. Gate opening $d=7.5\ cm$ and $H=22.5\ cm$.

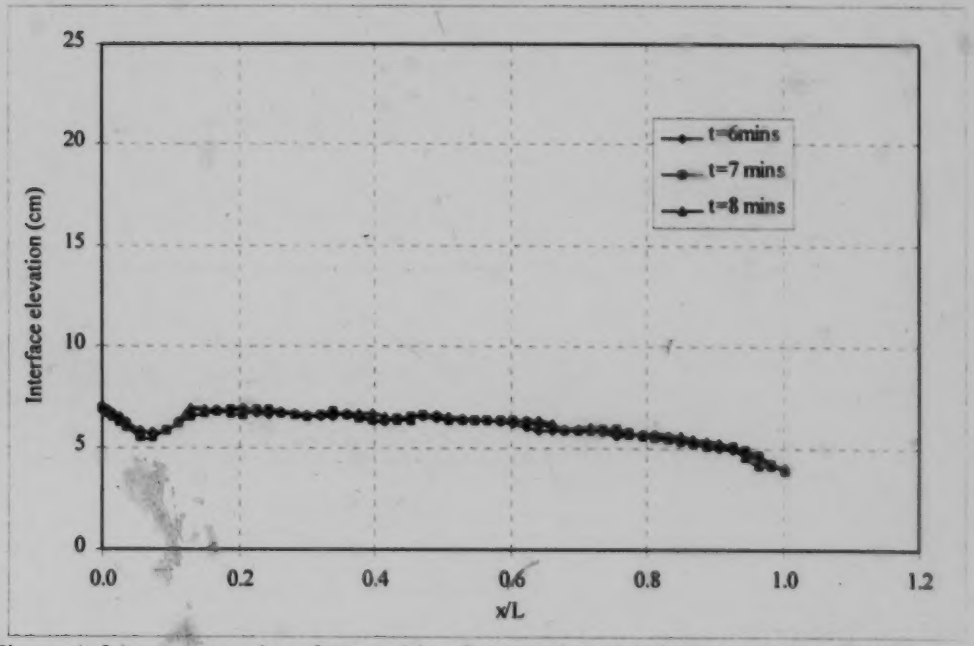

Figure A-24: Average interface position for experiment #12. Gate opening $d=7.5\ cm$ and $H=22.5\ cm$.

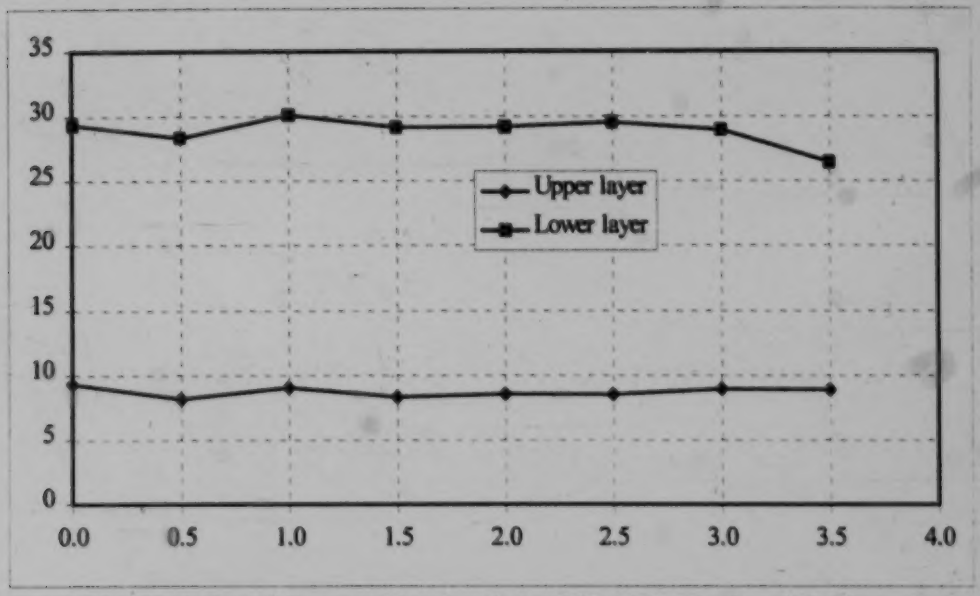

Figure A-25: Variation of flow rate for experiment #13. Gate opening *d=14.5 cm* and *H=22.5 cm.*

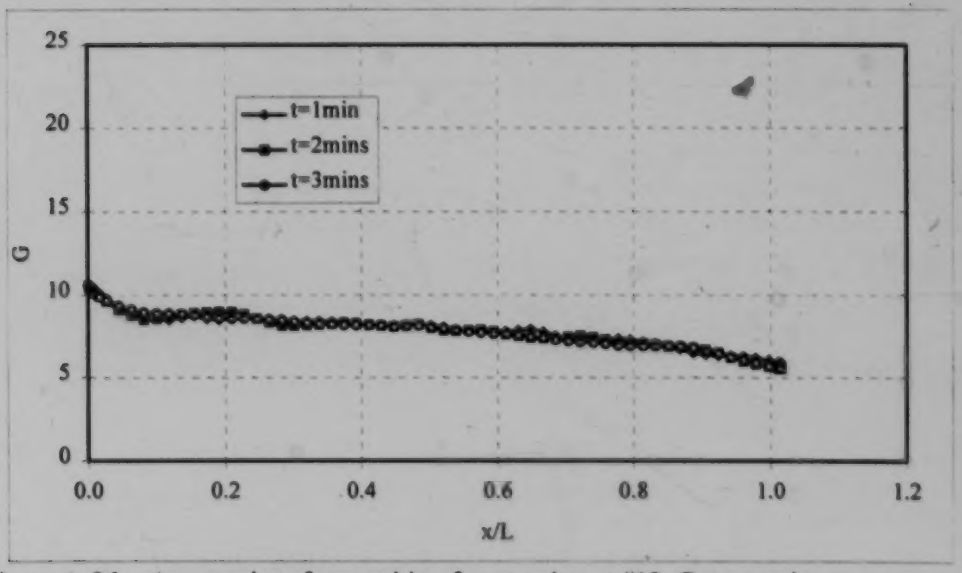

Figure A-26: Average interface position for experiment #13. Gate opening *d=14.5cm* and *H=22.5 cm.*